(2)

WL-TR-92-3043

AD-A252 101

WAVE PROPAGATION AND VIBRATION OF FIBRE-REINFORCED LAMINATES

W.A. Green
E. Rhian Green
G.A. Rogerson

Department of Theoretical Mechanics
The University,
Nottingham, NG7 2rd, UK

February 1992

Final Technical Report for Period 01 September 1988 to 30 September 1991

Approved For Public Release; Distribution Unlimited

FLIGHT DYNAMICS DIRECTORATE
WRIGHT LABORATORY
AIR FORCE SYSTEMS COMMAND
WRIGHT-PATTERSON AIR FORCE BASE, OHIO 45433-6553

NOTICE

When Government drawings, specifications, or other data are used for any purpose other than in connection with a definitely Government-related procurement, the United States Government incurs no responsibility or any obligation whatsoever. The fact that the government may have formulated or in any way supplied the said drawings, specifications, or other data, is not to be regarded by implication, or otherwise in any manner construed, as licensing the holder, or any other person or corporation; or as conveying any rights or permission to manufacture, use, or sell any patented invention that may in any way be related thereto.

This report is releasable to the National Technical Information Services (NTIS). At NTIS, it will be available to the general public, including foreign nations.

This technical report has been reviewed and is approved for publication.

Howard F. Wolfe

HOWARD F. WOLFE, Senior Engineer
Acoustics and Sonic Fatigue Group

Ralph M. Shimovetz

RALPH M. SHIMOVETZ, Group Leader
Acoustics and Sonic Fatigue Group

FOR THE COMMANDER

Jerome Pearson

JEROME PEARSON, Chief
Structural Dynamics Branch

If your address has changed, if you wish to be removed from our mailing list, or it the addressee is no longer employed by your organization please notify WL/FIBGD, WPAFB, OH 45433-6553 to help us maintain a current mailing list.

Copies of this report should not be returned unless return is required by security considerations, contractual obligations, or notice on a specific document.

REPORT DOCUMENTATION PAGE

Form Approved
OMB No. 0704-0188

1. AGENCY USE ONLY (Leave blank)	2. REPORT DATE	3. REPORT TYPE AND DATES COVERED
	5 February 1992	Final Technical Report 1 Sep 88 - 30 Sep 91

4. TITLE AND SUBTITLE
Wave Propagation and Vibration of Fibre-Reinforced Laminates

5. FUNDING NUMBERS
G-AFOSR-88-0353
PE 616200
PR 2302
TA N1
WU 06

6. AUTHOR(S)
W. A. Green, E. Rhian Green and G. A. Rogerson

7. PERFORMING ORGANIZATION NAME(S) AND ADDRESS(ES)
Department of Theoretical Mechanics
The University,
Nottingham, NG7 2RD, UK

8. PERFORMING ORGANIZATION REPORT NUMBER

9. SPONSORING/MONITORING AGENCY NAME(S) AND ADDRESS(ES)
Sponsoring Agency: WL/FIBGD, Howard Wolfe(513)2555229
Wright-Patterson AFB, OH 45433
Sponsoring/Monitoring Agency: European Office of Aerospace Research and Development
PSC 802, Box 14, FPO AE 09499-0200

10. SPONSORING/MONITORING AGENCY REPORT NUMBER
WL-TR-92-3043

11. SUPPLEMENTARY NOTES

12a. DISTRIBUTION/AVAILABILITY STATEMENT
Approved for public release:
distribution unlimited

12b. DISTRIBUTION CODE

13. ABSTRACT *(Maximum 200 words)*

Theoretical predictions are presented of the response of fibre-composite laminated plates to an impulse load. The cases considered were symmetric arrangements of four, six and eight plies of laminate consisting of straight parallel elastic fibres embedded in an isotropic elastic matrix. Analytical solutions allow the determination of the displacements and stress variation throughout the laminate at any time. The graphs presented show the variation of stresses and displacements along the plate surfaces and at the ply interfaces at fixed times. The analytical solutions illustrate the variation in the nature of the transmission with the direction of propagation and with ply lay-up. Surface impacts will initiate Rayleigh type surface waves propagating within a specified range of angles on any laminate. Outside this range of angles, the existence of the surface wave depends on the overall laminate depth. The study of these wave effects has thrown light on the way in which stress waves are channelled in the various layers of the laminate and on the manner in which this channelling is dependent on the angle between the fibre direction and the propagation direction in each layer.

14. SUBJECT TERMS
Wave Propagation, Vibration, Composites, Laminated Plates, Rayleigh Wave, Anisotropic Materials, Acoustic Emission, Interfacial Stresses

15. NUMBER OF PAGES
63

16. PRICE CODE

17. SECURITY CLASSIFICATION OF REPORT	18. SECURITY CLASSIFICATION OF THIS PAGE	19. SECURITY CLASSIFICATION OF ABSTRACT	20. LIMITATION OF ABSTRACT
UNCLASSIFIED	UNCLASSIFIED	UNCLASSIFIED	UL

FOREWORD

This report was prepared by The University of Nottingham, Nottingham, England for the Structural Dynamics Branch, Structures Division, Flight Dynamics Directorate, Wright Laboratory (WL/FIBG) Wright-Patterson Air Force Base, under Grant AFOSR-88-0353, Program Element 616200, Project 2302, Task Number N1, Work Unit Number 06. The work was administered under the direction of Howard F. Wolfe, WL/FIBGD. The monitoring officer in the UK was Lt Col James G.R. Hansen, EOARD/LDS. The program was conducted at the University of Nottingham, Department of Theoretical Mechanics, by Dr W.A. Green, Dr E. Rhian Green and Dr G.A. Rogerson. This report describes work conducted from 1 Sep 88 to 30 Sep 91.

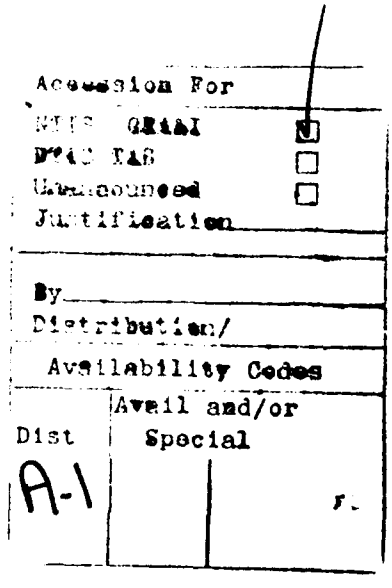

CONTENTS

LIST OF FIGURES

LIST OF FIGURES Cont'd

LIST OF FIGURES cont'd

LIST OF FIGURES cont'd

LIST OF FIGURES cont'd

LIST OF FIGURES Cont'd

LIST OF FIGURES Cont'd

1. INTRODUCTION

This work is concerned with the theoretical prediction of the response of fibre-composite laminated plates to impulsive events. Each layer of the laminate consists of a family of straight parallel elastic fibres embedded in an isotropic elastic matrix, forming a prepreg-ply. The plate is constructed by assembling these plies so that the fibre direction in each ply makes a specified angle with some reference direction. The results which are displayed here and in the preceding reports relate to symmetric arrangements of four, six and eight plies which are designated in the conventional nomenclature as $(90^0/0^0)_S$, $(-60^0/60^0/0^0)_S$, $(90^0/-45^0/45^0/0^0)_S$. Here the angles within the brackets denote the fibre orientation in each layer, starting from the outermost and moving in and the suffix s indicates that the plate is symmetric about its middle surface. In each case the fibre orientation in the inner (core) layer is chosen as the reference direction. The analytical solutions which are derived in this and the preceding reports allow the determination of the displacement and stress variation throughout the laminate at any time. In particular, they furnish information about the inter-ply stresses which is of immediate significance to the question of delamination. Numerical results are obtained from these analytical solutions and they are presented here in graphical form. The graphs show the variation of stresses and displacements along the plate surfaces and at the ply interfaces at fixed times. These are presented as examples of the wealth of information which it is possible to obtain from the analytic solutions and to illustrate the variation in the nature of the transmission with direction of propagation and with ply lay-up. Detailed solutions of this kind have not previously appeared in the literature and the work carried out on the project has led to a total of 15 publications in learned journals and conference proceedings.

The theoretical study of wave motion in laminated plates has been extensively pursued in recent years and surveys of the developments are presented in the review articles by Miklowitz [1], Ting [2], Pao [3] and Kapania and Raciti [4]. These accounts show that there exist a diversity of methods of approaching the problem but these can be classified into essentially three groups. One group involves making assumptions about the nature of the stress or displacement variation through the thickness of the laminate. This is the usual engineering mechanics

approach to plate theory and it allows the number of spatial variables to be reduced from three to two by integration through the thickness. Examples of the use of this technique to study impact problems are contained in the papers by Chow [5], Moon [6] and Sun [7]. The hybrid numerical method described by Lui et al [8] can also be regarded as an example of this technique. In this hybrid method the finite element formalism is employed to express the variation through the thickness in terms of displacements on a finite number of planes within the plate and the problem is thus reduced to solving equations of motion involving two spatial dimensions on each of these planes. The second group of methods employs a purely numerical approach to solving the problem and examples are furnished in the paper by Lee et al [9] and the paper by Wu and Springer [10]. These both employ the finite element numerical technique to evaluate the transient stresses induced by impact on composite plates.

Solution methods which belong in either of the two groups described above will of necessity lead only to approximate results, since by their nature they are incapable of reproducing the details of the stress variation throughout the laminate thickness. For low frequency vibrations, or for transient motion due to low velocity impact, where the wavelength of the disturbance is large in comparison with the overall plate thickness, these methods could be expected to provide good results. High velocity impacts and internal impulsive events such as delamination or cracking, on the other hand, will give rise to transient motion involving a wide range of frequencies (and wavelengths). For these, the stress variation through the laminate thickness may well differ significantly from that assumed in the approximate theories and it becomes necessary to analyse these problems using the full three dimensional equations of elasticity. It is methods which make use of these full elasticity equations which constitute the third group of solution techniques. Examples are provided in the work of Miklowitz [11], Ceranoglu and Pao [12], Weaver and Pao [13], Vasudevan and Mal [14] and Willis and Bedding [15]. These methods generate the exact analytic solutions using transform techniques [11,14,15], the method of generalised rays [12] and the method of normal modes [13]. With these solutions it becomes possible to evaluate stress and displacement components at any location within or on the surfaces of the plate with the only approximation being that arising from the procedure for numerical

computation of the analytic solution. It is this three dimensional approach that has been adopted in the work which is reported here.

That the details of the stress variation throughout the laminate have a practical significance is illustrated in a recent paper by Stone and Chatterjee [16] dealing with the effect of multiple impacts on laminated plates. These authors showed that the directional focusing of waves arising from the first impact could cause weakening of the inter-ply bonds at regions away from the immediate impact site, with the weakened regions suffering delamination as a result of subsequent impacts. In the work reported here it is assumed that the plate maintains its structural integrity during and after the impact process and in consequence the results are not valid in the immediate impact region when the magnitude of the event is such as to cause fracture or delamination of the material. Despite this, the results of this work remain valid in those regions for which no damage occurs, since it is possible to model the effects of the processes occurring in the damaged region by an equivalent spatial distribution of time dependent sources in a manner analogous to that employed in seismology to model the effects of internal events which give rise to earthquakes.

In addition to their immediate relevance to the problem of impact, these results are of importance in the quantitative non-destructive evaluation (QNDE) process. The QNDE technique of acoustic emission employs the stress waves generated by internal cracks or delaminations under an applied load as a means of determining the location and extent of internal flaws within structural members. The interpretation of acoustic emission events monitored on the surface relies on a detailed knowledge of the mode of transmission of the stress waves through the structure and the work reported here provides this detailed knowledge for multi-ply fibre composite materials. The techniques which have been developed may be applied to more general lay-ups and to more plies than those that have been employed here for illustrative purposes. Of particular relevance to the acoustic emission application is the recent work of Sachse and co-workers [17] who have developed a neural network type intelligent learning system for the interpretation of acoustic emission events. This system has been shown to have the capability of reconstructing the source characteristics of a non-standard internal event from partial information, after exposure to a set of standard known events in the learning

process. The results obtained through the research grant provide the basic information which is required in the learning process for laminated plates.

In carrying out the analysis which is the subject of this report it has been assumed that the plies which form the laminate are perfectly bonded to each other so that the displacement and tractions are continuous across each interface. The material forming each of the plies has been modelled as a transversely isotropic homogeneous elastic continuum in which the axis of transverse isotropy is parallel to the fibre direction The elastic properties of a transversely isotropic material involve five independent elastic constants. The results reported here have been derived using numerical values for these constants which relate to a particular carbon fibre/epoxy resin matrix composite studied by Markham [18]. In adopting the homogeneous continuum model for the fibre composite, it is assumed that the wavelengths of the disturbances are large in comparison with the fibre diameter and inter-fibre spacing. For typical prepreg-plies containing some 60% by volume of fibre, the fibre diameter and inter fibre spacing is of the order of 6 μm with the ply thickness being approximately 120 μm. The assumption of homogeneity might be expected to be valid in such a material for wavelengths of the order of 1/3 the ply thickness or greater. On the other hand, for wavelengths of order 1/10 the ply thickness or less, the waves would suffer diffraction and scattering by the individual fibres and the homogeneous continuum model would no longer hold. For the material constants employed here, this implies that the continuum model should be expected to hold at frequencies up to approximately 30 MHz.

The analytic solutions have been derived for impulsive loads which are represented mathematically by a Dirac delta function of time. An impulse of this kind has a constant spectrum, indicating that all frequencies from zero to infinity occur with equal amplitude. Whilst such a function is physically unrealistic the response generated by it constitutes the fundamental (Green's function) solution from which it is possible to obtain the response of the laminate to any impulse with any other time history by means of a convolution. The majority of graphs displayed in this report relate to the response to this delta function loading, but some examples are also included which display the response to more physically meaningful time dependent loads. Time varying loads of finite duration generally have non-zero spectra over a finite range of frequencies and the upper frequency

limit of 30 MHz for which the continuum model is valid is associated with loads having a significant variation over times of the order of 10^{-8} sec. Whilst time variations of this order can arise in laser generated impact pulses the time variation associated with more conventional impacts will be orders of magnitude greater than this and the wavelengths associated with such impacts will be well within the range of validity of the continuum model.

All the work carried out in this project relates to a line load impulse acting either on the upper plate surface or at one of the interfaces between plies. The interfacial line load impulse provides the basic solution associated with a delamination at the interface, whilst the upper surface line load impulse provides the basic solution for the surface impact problem. The laminated plates have been assumed to have infinite lateral extent so that the results relate to waves propagating outwards from the impulse location. In a realistic situation, the results remain valid at any point up to the time of arrival of disturbances reflected from the plate edges. Reflection from the edge of a plate can be modelled by a distribution of time dependent loads along the edge which are such as to satisfy the edge conditions when added to the incident wave. These balancing loads will initiate disturbances travelling back into the plate which, when added to the original disturbance, will yield the solution for plates of finite lateral dimensions.

The impulses employed to generate these solutions were assumed to act along a line of infinite length and to be of uniform strength along the line. An impulse of this kind would set up a disturbance travelling away from the line through the laminate in such a way that the solution would be identical in every plane perpendicular to the impulse line. The analytic solutions are consequently independent of position along the line and are functions of two space variables and the time only. For isotropic materials the displacements would be confined to lie in the planes perpendicular to the impulse line but this is not the case for the anisotropic materials which have been studied here. The solutions involve all three components of displacements and all six components of stress, despite the fact that these are all functions of two space variables only. The use of line load impulses was adopted as a first step toward the ultimate goal of determining the response to a point load. In an infinite body of isotropic material, for which the speeds of elastic waves are independent of orientation, the response to a point load would be

spherically symmetric disturbances travelling outwards from the point of initiation. This would not be the situation for anisotropic materials, where waves travel with different speeds in different directions. Even for isotropic materials, the propagation due to point sources in plates and/or laminates, which is brought about by reflection and transmission of waves at the interfaces and reflection at the outer surfaces, presents a formidable problem. This problem is even more formidable for anisotropic laminates and the method of approach which was adopted in this project was to make use of the fact that the point load solution could be generated by a suitable integration of line load solutions taken over all possible orientations of the line load relative to some reference direction. With this aim in mind the project has dealt with the generation of line load solutions for different orientations of the line load.

The basic method of solution has been to take Laplace Transforms with respect to time and Fourier Transforms with respect to one of the spatial variables, so as to reduce the governing equations to a coupled system of linear ordinary differential and algebraic equations for the transforms of the displacement components and the stress components in terms of the variable measuring distance through the laminate. These equations have different forms within each of the plies and the solution within each ply has been derived in terms of the propagator matrix for that ply. Continuity of displacements and traction components between each ply leads to the solution for the stress and displacement transforms in terms of an overall propagator matrix for the laminate as a whole and the transform of the impulsive load. In order to recover the solution as functions of position and time, it is necessary to invert the transforms and this process has been performed numerically.

In an attempt to reduce both the mathematical and numerical complexity of the problem, the first approach adopted a simplified model of the fibre composite plies in which the transversely isotropic model material was assumed to be inextensible in the fibre direction. Earlier work by Green [19] and Baylis and Green [20] had demonstrated that this inextensible model showed good agreement with the more realistic extensible model material over a large range of wavelengths, with the differences becoming apparent only at very long wavelengths and at very short wavelengths. The assumption of inextensibility had been widely employed in

modelling equilibrium deformations of fibre composites (see eg. Spencer [21]) where it had been shown to give rise to a considerable simplification in the governing equations. In the dynamic problem, likewise, this model led to a simplification in that the governing equations within each ply reduced from a system of six first order ordinary differential equations to a system of four first order ordinary differential equations. A further simplification, arising from the continuity conditions at the interfaces between plies, yielded the solution to the problem for the laminate in terms of an overall propagator matrix of order 2. This matrix consisted of a product of (2×2) matrices, one for each ply, whereas, for the extensible model the solution involved an overall propagator matrix of order 6, formed as a product of (6×6) matrices.

The initial set of results related to a four layer symmetric cross-ply $(90^0/0^0)_S$ laminate and were derived using the inextensible model for each ply. Analytic solutions for the transforms of displacements and stress components have been obtained for the delta function line load acting on the top surface of the plate, with the line making an arbitrary angle γ with the fibre direction in the outer layers. The resulting wavefront moves in a direction at right angles to the line load and making angle γ with the fibre direction in the core layers. Numerical results were calculated for angles of propagation $\gamma = 0^0, 30^0, 45^0, 60^0, 90^0$. These results were displayed as graphs showing the variation of displacement or stress components as a function of distance from the impulsive line along the direction of propagation at fixed times. Whilst it is possible to obtain values at any level in the laminate, the locations of particular interest are the ply interfaces, the middle plane and the outer surfaces of the plate. These first results showed a striking phenomenon. This related to the presence of a strong Rayleigh-type surface wave travelling along the impacted upper surface for a range of values of the propagation angle γ and the absence of any surface wave for propagation at angles outside the range. The explanation of this phenomenon is to be found in the behaviour of the dispersion equations for the propagation of time harmonic waves in the laminate under traction free conditions on its outer surface. In particular, the existence or non-existence of the surface wave was shown to be associated with the limiting short wavelength behaviour of the fundamental mode of the dispersion equations. This is discussed in detail in the body of this report.

Following the success of the technique for the four-ply laminate, the inextensible model was subsequently employed to generate the analytic transform solutions for the six-ply $(-60^0/60^0/0^0)_S$ and the eight-ply $(90^0/-45^0/45^0/0^0)_S$ laminates. Here again, numerical transform inversion was carried out to determine displacements and stresses associated with angles of propagation $\gamma = 0^0, 30^0, 45^0, 60^0, 90^0$ relative to the fibre direction in the core, for both lay-ups. Some of these results indicated the existence of Rayleigh-type surface waves propagating at angles for which no surface wave would have existed in the four-ply case, Subsequent investigation showed that this unexpected occurrence was associated with the behaviour of the higher modes of the dispersion equations at intermediate wavelengths. The study of these surface wave effects has thrown light on the way in which the stress waves are channelled in the various layers of the laminate and on the manner in which this channelling is dependent on the angle between the fibre direction and the propagation direction in each layer.

The next stage in the investigation was to relax the constraint of inextensibility and in the first instance this was done on the four layer cross-ply plate. The solution procedure which was adopted was to take Laplace and Fourier transforms as before. This reduced the governing equations to a system of six coupled ordinary differential equations within each ply, whose solutions were expressed in terms of a (6×6) propagator matrix in each ply. Continuity at the ply interfaces allowed the solution throughout the laminate to be expressed in terms of an overall propagator matrix of order six, formed as a product of the individual propagators for each ply. The imposed loading conditions at the top surface, together with the traction free conditions at the bottom surface then yielded the analytic solutions for the transformed components of displacements and stresses. Whilst the propagator matrix method produced the analytic solution for the transforms in a compact form, it turned out that the use of this compact form for numerical inversion of the transforms led to considerable computational problems. These problems arose because at large values of the wavenumber k (short wavelengths) the individual propagators contain positive exponentials which grow with increasing wavenumber. In the analytic solution these large exponential values cancel out. However, because of rounding effects inherent in any computation, they give rise to precision problems in the numerical inversion. In an attempt to

overcome this numerical problem Green [23] has adapted an alternative solution due to Mal [23] and has succeeded in obtaining numerical results for the four-ply laminate.

When the displacement components in the direction normal to the plate, calculated using the extensible model, are compared with those derived using the simplifying assumption of fibre inextensibility they show significant discrepancies. These arise from the inability of the simplified model to reproduce the correct behaviour of the plate in the long wavelength limit. In the long wavelength limit the extensible model displays the correct St. Venant bending behaviour associated with classical plate theory. The inextensible model is incapable of reproducing a pure bending deformation and it yields a shearing behaviour of the laminate in the long wave limit. Despite this inconsistency of the displacement components, the stress components derived from the two models show very good agreement. This is because the stresses derive mainly from the shorter wavelength components of the disturbance where the two models exhibit similar behaviour. On this basis it would be reasonable to conclude that the inextensible model should provide an acceptable representation of the transient stress level arising from impulsive events. Further applications of the extensible model have been carried out in order to evaluate the response due to internal impulsive events arising at the interfaces between the plies in the four-ply plate. These have demonstrated the usefulness of the technique for predicting the effect both of surface impacts and internal cracking or delamination.

In the Green-Mal technique which has been employed to derive the response of the four-ply extensible model, the formal analytic solution is expressed in terms of the inverses of two matrices, each of order 12. The calculation of the graphical results then involves a numerical integration along branches of the dispersion curves which relate frequency to wavenumber. These curves are obtained by setting the determinant of each (12×12) matrix equal to zero and solving for the frequencies at a specified set of values of wavenumber. The technique is such that no element of these matrices involves exponentials with positive real parts and the precision problems which arise in the propagator matrix method are eliminated at the expenses of increasing the order of the determinants from 6 to 12. The application of the approach to symmetric plates with more than four layers involves increasing the order of the matrix in the solution by 6 for each pair of layers. Thus the 6-ply

plate involves two matrices, each of order 18, whilst the 8-ply plate involves two matrices, each of order 24. In both cases, the propagator matrix is of order 6 and the precision problems are eliminated at the expense of increasing the order of the matrix. The computational effort involved in solving the dispersion equations is proportional to the cube of the order of the matrix so that the 6-ply plate requires more than three times the computer time needed for the 4-ply plate, with this factor increasing to eight times for the 8-ply plate. In consequence, the extension of the method has been carried out for the six-ply plate only and even here the computation problem has had to be reduced by adopting a cross-ply $(0^0/90^0/0^0)_S$ lay-up, rather than the $(-60^0/60^0/0^0)_S$ configuration which was studied when using the inextensible model. Nevertheless, the results for this six-ply laminate, when compared with those for the four-ply, do furnish information concerning the effect of increased layering which supports the conclusions arrived at in studying the inextensible model.

The remainder of this report is divided into four sections. Section 2 is concerned with deriving the analytic solutions using both the propagator matrix method and the Green-Mal approach. The method of transform inversion is outlined in Section 3 and Section 4 is devoted to the presentation of results. In view of the fact that this constitutes the final report on the project, Section 4 is subdivided into four subsections. Of these subsections, the first (subsection (a)) consists of a synopsis of the results contained in the report on the preliminary program, carried out under Grant #AFOSR-86-0330. The second (subsection (b)) is a summary of the contents of the first scientific report on the present project, the third (subsection (c)) outlines the contents of the second scientific report and the final subsection (d) deals with the results obtained subsequent to the second report. Section 5 consists of a discussion of the results as a whole, together with the conclusions arising from the project.

2. ANALYTIC SOLUTION

The problem which has been examined is illustrated in Figure 1. This shows a symmetric arrangement of $2n$ plies with a system of coordinates axes $Ox_1x_2x_3$ chosen such that the mid-surface of the laminate is the plane $x_3 = 0$, with the upper surface at $x_3 = nh$ and the lower surface at $x_3 = -nh$, where h is the individual ply

thickness. The layers are shown numbered in the upper half plate with the inner laye. numbered 1 and the outer layer n. The line load impulse is taken to be acting on the upper surface $x_3 = nh$ along the line parallel to the x_2-axis and in the direction of the inward normal. This generates a disturbance travelling through the plate in such a way that the displacement components u_i and the stress components t_{ij} $(i,j = 1,2,3)$ are functions of the coordinates x_1, x_3 and of the time t only and have no dependence on the coordinate x_2. In order to derive the analytic solution it is convenient to take the Laplace transform with respect to time and the Fourier transform with respect to the x_1 coordinate of all the components of displacement and stresses . This gives the functions $U_i(k,x_3,s)$, $T_{ij}(k,x_3,s)$ defined by

$$U_i(k,x_3,s) = \int_{-\infty}^{\infty} \int_0^{\infty} u_i(x_1,x_3,t)\, e^{ikx_1}\, e^{-st}\, dt\, dx_1$$

$$T_{ij}(k,x_3,s) = \int_{-\infty}^{\infty} \int_0^{\infty} t_{ij}(x_1,x_3,t)\, e^{ikx_1} e^{-st}\, dt\, dx_1 . \qquad (1)$$

The governing equations consist of the equations of motion under no body forces together with the stress/strain relations and the equations relating the strain components to the derivatives of the displacement components. Of these, the equations of motion and the relations between strain and displacement gradients have the same form throughout the laminate whilst the stress/strain relations involve different elastic constants in each layer. The plate is assumed to consist of identical layers of a fibre composite material arranged so that the fibre direction in layer m makes a specified angle ψ_m with the direction of the x_1-axis. The elastic constants in layer m may be expressed in terms of the five elastic constants of the transversely isotropic material forming each ply, together with the orientation angle ψ_m of the layer. When the governing equations have been subjected to the same transform operations as the displacement and stress components, there results a coupled system of six ordinary differential equations in each layer, which, for layer m, may be written in the form

$$\frac{dY}{dx_3} = ik A_m Y . \qquad (2)$$

Here A_m is a (6×6) matrix whose elements are functions of the elastic constants of layer m and of the transform parameters k and s and Y is the six vector $(U_1\, U_2 U_3 T_{13} T_{23} T_{33})^{\mathrm{T}}$ with T denoting the transpose. The remaining transformed

components of stress in layer m can be written in terms of the elements of Y in the form

$$X = B_m Y \tag{3}$$

where $X = (T_{11} T_{12} T_{22})^T$ and B_m is a (3×6) matrix whose elements are given in terms of the elastic constants of layer m and the transform parameters.

Propagator Method

Equations (2) have the general solution

$$Y_m(z_m) = P_m(z_m)\, Y_m(0)\,, \tag{4}$$

where $z_m = x_3 - (m-1)h$, $Y_m(z_m) \equiv Y(x_3)$ and $P_m(z_m)$ is the propagator matrix for layer m. The condition of perfect bonding between each of the plies ensures that the vector $Y(x_3)$ is continuous at the interface between any two plies so that

$$Y(mh) = Y_{m+1}(0) = Y_m(h)\,, \qquad m = 1, 2, \ldots (n-1)\,. \tag{5}$$

The repeated use of equations (4) and (5) gives the solution in layer m in terms of the vector $Y(0)$ at the mid-surface in the form

$$Y(x_3) = P_m(z_m)\, P_{m-1}(h) \ldots P_1(h)\, Y(0)\,. \tag{6}$$

Applying equation (6) to the complete upper half plate gives

$$Y(nh) = P\, Y(0)\,, \tag{7}$$

where $P = P_n(h)\, P_{n-1}(h) \ldots P_1(h)$, is the overall propagator matrix for the half plate.

The boundary conditions to be satisfied at the top and bottom surfaces of the plate are

$$\begin{aligned} &t_{13} = t_{23} = 0\,, \quad t_{33} = -\delta(x_1)\,\delta(t) && \text{at } x_3 = nh \\ &t_{13} = t_{23} = t_{33} = 0 && \text{at } x_3 = -nh \end{aligned}$$

where $\delta(.)$ is the Dirac delta function. Taking Laplace and Fourier transforms of these yield the conditions

$$\begin{aligned} &T_{13} = T_{23} = 0 \quad T_{33} = -1 && \text{at } x_3 = nh \\ &T_{13} = T_{23} = T_{33} = 0 && \text{at } x_3 = nh\,. \end{aligned} \tag{8}$$

These boundary conditions may be replaced by the two sets of boundary conditions

$$T_{13} = T_{23} = 0 \quad T_{33} = -\tfrac{1}{2} \qquad \text{at } x_3 = \pm nh\,, \tag{9a}$$

and

$$\begin{aligned} &T_{13} = T_{23} = 0 \quad T_{33} = -\tfrac{1}{2} && \text{at } x_3 = nh\,, \\ &T_{13} = T_{23} = 0 \quad T_{33} = +\tfrac{1}{2} && \text{at } x_3 = -nh\,. \end{aligned} \tag{9b}$$

Because of the linearity of the governing equations the solution to the problem subject to the boundary conditions (8) may be obtained by adding together the solutions to the problem with boundary conditions (9a) and the solution to the problem with boundary conditions (9b). This apparent doubling of the work involved does in reality yield an overall reduction, since the symmetry of the plate, together with the symmetry of the boundary conditions (9a) and the anti-symmetry of the boundary conditions (9b) mean that each of these problems can be solved by solving the equations in the upper half plate only.

For the symmetric problem (9a), the solution vector $Y_s(-x_3)$ at any level in the lower half plate is given in terms of the solution vector $Y_s(x_3)$ at the corresponding level in the upper half plate by the relation

$$Y_s(-x_3) = M_s\, Y_s(x_3). \tag{10a}$$

where M_s is the diagonal matrix defined by $M_s = \text{diag}\,(1, 1, -1, -1, -1, 1)$. For the anti-symmetric problem (9b) the solution in the lower half plate $Y_a(-x_3)$ is given in terms of the solution $Y_a(x_3)$ at the corresponding level in the upper half plate, by the expression

$$Y_a(-x_3) = M_a\, Y_a(x_3). \tag{10b}$$

and the diagonal matrix M_a is defined by $M_a = \text{diag}\,(-1, -1, 1, 1, 1, -1)$. Equations (10a) and (10b) yield the boundary conditions to be satisfied by the vector $Y(0)$ at the mid-surface for the symmetric and the anti-symmetric problems respectively as

$$U_3^s(0) = 0\,, \quad T_{13}^s(0) = 0\,, \quad T_{23}^s(0) = 0\,, \tag{11a}$$

$$U_1^a(0) = 0\,, \quad U_2^a(0) = 0\,, \quad T_{33}^a(0) = 0\,. \tag{11b}$$

Substituting the boundary conditions (9a) and (11a) into equations (7) leads to expressions for the non-zero mid-plane components $U_1^s(0)$, $U_2^s(0)$, $T_{33}^s(0)$, of the symmetric vector $Y_s(0)$ and using the boundary conditions (9b) and (11b) leads to the non-zero antisymmetric components $U_3^a(0)$, $T_{13}^a(0)$, $T_{33}^a(0)$. Adding these gives the mid-surface vector $Y(0)$ which is associated with the solution of the original problem (boundary equations (8)) from which, the solution at any point $x_3 = z_m + (m+1)h$ in the upper half plane may be obtained on using the expression (6). The mid-surface vector $Y(0)$ has the form

$$Y(0) = \left(\frac{m_1}{D_S} \; \frac{m_2}{D_S} \; \frac{m_3}{D_a} \; \frac{m_4}{D_a} \; \frac{m_5}{D_a} \; \frac{m_6}{D_S} \right)^{\mathrm{T}}, \tag{12}$$

where $m_1, m_2, \ldots, m_6$ are known functions of the elements of the overall propagator matrix P. D_S and D_a are the 3×3 determinants defined by

$$D_S = \begin{vmatrix} p_{11} & p_{12} & p_{16} \\ p_{21} & p_{22} & p_{26} \\ p_{31} & p_{32} & p_{36} \end{vmatrix}, \qquad D_a = \begin{vmatrix} p_{13} & p_{14} & p_{15} \\ p_{23} & p_{24} & p_{25} \\ p_{33} & p_{34} & p_{35} \end{vmatrix}, \tag{13}$$

and p_{ij} are the elements of P. The solutions presented here relate to waves propagating along the x_1-axis but it is straightforward matter to derive the solution for propagation at any angle γ to the x_1-axis. This is done by choosing a new system of axes $Ox_1' x_2' x_3'$ so that Ox_1' coincides with the propagation direction and the solution relative to this system of axes is then derived from the present solution on replacing the angle ψ_m by $(\psi_m - \alpha)$ for $m = 1, 2, \ldots, n$.

Direct Matrix Method

It has been remarked in Section 1 that the propagator matrix method described above can give rise to numerical difficulties in the transform inversion because of the presence of exponentials with large positive arguments. An alternative method originally introduced by Mal [23] has been adapted by Green [22] and employed in an attempt to overcome these numerical difficulties. In this method, the solution of the differential equations (2) in layer m are written in the form

$$Y(z_m) = D_m \, E_m(z_m) \, C_m \, . \tag{14}$$

where D_m is a constant matrix whose columns are the eigenvectors of the matrix A_m of equations (2). C_m is a vector of arbitrary constants and $E_m(z_m)$ is the diagonal matrix defined by

$$E_m(z_m) = \mathrm{diag}\left\{ e^{ikp_1^m z_m}, \; e^{ikp_2^m z_m}, \; e^{ikp_3^m z_m}, \; e^{-ikp_1^m (z_m - h)}, \right.$$
$$\left. e^{-ikp_2^m (z_m - h)}, \; e^{-ikp_3^m (z_m - h)} \right\},$$

and $\pm p_1^m, \pm p_2^m, \pm p_3^m$ are the eigenvalues of A_m. This choice of E_m ensures that whenever one of p_α^m ($\alpha = 1, 2, 3$) is imaginary, the two corresponding entries in E_m give rise to decaying exponentials for $0 \le z_m \le h$. Making use of the solutions (14) in layers m and $(m+1)$ and substituting into the interface continuity conditions gives

the relations

$$D_{m+1}\, E_{m+1}(0)\, C_{m+1} - D_m\, E_m(h)\, C_m = 0 \qquad (15)$$

Equations (15) hold at each interface $m = 1, 2, \ldots (n-1)$ and they constitute a system of $6(n-1)$ equations in the $6n$ unknowns which appear in the vectors $C_1, C_2, \ldots C_n$. The remaining 6 equations are obtained from the boundary condition at the midsurface $x_3 = 0$ and at the upper surface $x_3 = nh$. These are the conditions (11a) and (9a) for the symmetric solutions and the conditions (11b) and (9b) for the antisymmetric motion. In each case, equations (15) for $m = 1, 2, \ldots, n-1$ together with the six boundary conditions (3 at $x_3 = 0$ and 3 at $x_3 = nh$) give a system of $6n$ linear simultaneous equations for the $6n$ constants $C_1, C_2, \ldots, C_m$ which have the matrix forms

$$H_s\, C^s = B_s\,, \qquad H_a C^a = B_a\,, \qquad (16)$$

where H_S, H_a are $(6n \times 6n)$ matrices whose elements are known, B_s and B_a are each $6n$ column vectors associated with the boundary conditions and C^s and C^a are the $6n$ column vectors of arbitrary constants which are to be determined for the symmetric and antisymmetric solutions respectively. The solutions of equations (16) for C^s and C^a are added to give the upper half plate vectors of constants $C_1, C_2, \ldots C_n$ which then yield the vectors $Y(z_m)$ at any point on using equations (14). The solutions of equations (16) may be written in the form

$$C^s = H_s^{-1} B_s = \frac{(\text{Adj } H_s)}{(\det H_s)}\, B_s\,, \qquad C^a = H_a^{-1} B_a = \frac{(\text{Adj } H_a)}{(\det H_a)}\, B_a\,, \qquad (17)$$

where the inverse matrices H_s^{-1} and H_a^{-1} are expressed in the form of the adjoint matrices (Adj H_s), (Adj H_a), divided by the determinants (det H_s) and (det H_a) respectively. Since the elements of the matrices H_s and H_a are derived from those of the individual layer matrices $D_m\, E_m(0)$ and $D_m\, E_m(h)$, they involve no growing exponential terms which would be a potential source of numerical instability.

3. TRANSFORM INVERSION

Either of the two analytic methods outlined in the previous Section will yield expressions for the transformed components of displacements or stresses at any level in the plate. These are functions of x_3 and of the transform parameters k and s. They all have the form N/D where the numerator N is a function of x_3, k and s and the denominator D is a function of k and s only. There is a different numerator

N for each transformed component of displacement or stress but the denominator D is the same for all components. In the propagator matrix method this denominator is one of the 3×3 determinants defined in equations (13) whereas in the direct matrix method the denominator D is a determinant of order $6n \times 6n$ as shown in equation (17). The formal inversion of the typical component of stress or displacement is given by the expression

$$f(x_1, x_3, t) = \frac{1}{4\pi^2 i} \int_{-\infty}^{\infty} \int_{\gamma - i\infty}^{\gamma + i\infty} \frac{N(k, x_3, s)}{D(k, s)} e^{st} e^{-ikx_1} \, ds \, dk , \tag{18}$$

where $f(x_1, x_3, t)$ represents the stress or displacement component.

The integral with respect to s is evaluated using the theory of residues. For a fixed value of k the denominator $D(k, s)$ has an infinite number of roots located at the points $s = \pm i\omega_j$ $(j=1,2,\ldots)$ along the imaginary s axis and which satisfy the equation

$$D(k, \pm i\omega_j) = 0 \qquad j = 1, 2, \ldots \tag{19}$$

This equation is identical with the dispersion equation which relates the frequency ω to the wavenumber k for harmonic waves, propagating along the x_1-direction in the plate, under traction free conditions on the outer surfaces. The roots $s = \pm i\omega_j(k)$ $(j=1,2,\ldots)$ correspond to the different branches of this dispersion equation. The residue $R_j(k, x_3)$ associated with the root of the denominator at $s = i\omega_j(k)$ is given by

$$R_j(k, x_3) = \frac{N(k, x_3, i\omega_j(k))}{\left\{dD/ds\right\}_{s = i\omega_j}} . \tag{20}$$

It is straightforward to show that both N and D depend on the parameter s only through its square (s^2) and it then follows that the residue associated with the root $s = -i\omega_j(k)$ is $-R_j(k)$. Making use of these results, equation (18) may be written as

$$f(x_1, x_3, t) = \frac{1}{\pi} \int_{-\infty}^{\infty} \left\{ \sum_{j=1}^{\infty} R_j(k, x_3) \sin\omega_j(k) t \right\} e^{-ikx_1} \, dk , \tag{21}$$

This involves an infinite integral of an infinite sum and it is at this stage that approximations are introduced in order to obtain numerical results. These approximations consist of restricting the range of integration to be finite $(-\hat{k}, \hat{k})$ and carrying out the summation over a finite set of values of j $(j=1, \ldots, P)$. In all the numerical results, the value of $\hat{k}$ has been chosen to be $20/h$, which corresponds to

the smallest wavelength being approximately one third the ply thickness h. For wavelengths below this value, the effects of diffraction and scattering by the individual fibres in the composite might be expected to become significant, as has been indicated in Section 1 of this report. Thus, the choice of $\hat{k} = 20/h$ is consistent with the representation of the composite material as a homogeneous continuum. All the results have been calculated by summation over a total of 20 branches of the dispersion equation, these being the first ten branches of each of the symmetric and the antisymmetric modes.

In order to obtain the detailed results it is therefore necessary to solve the dispersion equation (19) numerically and to evaluate the residues defined by equation (20) for values $j=1, 2, \ldots, 20$. Details of the numerical procedures have been given in the earlier reports and they will not be reproduced here.

4. RESULTS

Whilst the analytic solutions which are presented in Section 2 are valid for all fibre composite laminates, for the purpose of evaluating the solutions numerically it is necessary to specify the values of the elastic constants. For all the results that are reported in this project the values chosen have been those obtained experimentally by Markham [18]. These values relate to a carbon fibre/epoxy resin composite which is modelled as a transversely isotropic elastic material. These values are such that the extensional modulus of the material parallel to the fibre direction is of the order of 25 times that in any direction at right angles to the fibre. In the usual double suffix extended notation for anisotropic elasticity these constants are

$$c_{11} = 241.71\ GP_a\,, \quad c_{22} = c_{33} = 10.57\ GP_a\,, \quad c_{21} = c_{31} = 4.37\ GP_a\,,$$

$$c_{23} = \ \ 5.65\ GP_a\,, \quad c_{44} = \tfrac{1}{2}(c_{22} - c_{23})\,, \qquad c_{55} = c_{66} = 5.66\ GP_a\,.$$

These values are used solely for the purpose of illustration and they have been employed because they have been established under controlled experimental conditions. Their relative magnitudes are consistent with values quoted by suppliers of commercially available prepregs and the results are therefore believed to be representative of the transmission of impact stress waves in such materials. Using these constants, it is convenient to define reference wave speeds c_1, c_2, c_3, c_4, c_5 given

by the relations $\rho c_1^2 = c_{22}$, $\rho c_2^2 = c_{44}$, $\rho c_3^2 = c_{55}$, $\rho c_4^2 = c_{21}$, $\rho c_5^2 = c_{11}$, where ρ is the density of the material. The ratios of these wave speeds are independent of the density ρ and all results are given in terms of these ratios, with the stress components being scaled by the modulus c_{22}.

This Section is divided up into 4 sub-sections of which the first three consist of resumés of the results contained in the report of Grant # AFOSR-86-0330 (Section 4(a)), in the first interim report on the current Grant # AFOSR-88-0353 (Section 4(b)) and in the second interim report on the current grant (Section 4(c)). The final sub-section (4(d)) deals with the results obtained subsequent to the second interim report.

4(a) Grant # AFOSR-86-0330

The work carried out under this initial grant dealt solely with the four-ply plate in which each ply was modelled as a homogeneous transversely isotropic elastic medium which was assumed to be inextensible in the fibre direction. This simplified model was adopted with the object of reducing the mathematical complexity so as to allow the potential of the approach to be evaluated within the one year time period of the grant.

The results presented in the report on this grant fell into 3 groups. The first group consisted of plots of the dispersion curves for the first nine branches of symmetric and of antisymmetric motion for time harmonic waves propagating under traction free conditions on the laminate surfaces. These dispersion curves show the variation of circular frequency ω with wave number k and they are obtained by numerical solution of equation (19) using the expression for $D(k,s)$ which is appropriate to the symmetric and the antisymmetric motions of the four-ply plate. Results were presented for propagation at angles 0^0, 30^0, 45^0, 60^0 and 90^0 relative to the fibre direction in the core. Figure 2 is a copy of Figure 1 of the original report and it shows a set of 26 dispersion curves for propagation at angle $\gamma = 90^0$. These consist of the first 13 modes of both the symmetric and antisymmetric motion and they have been plotted together in order to display the phenomenon of ghost lines, brought about by osculation of the branches. These ghost lines correspond to a phase velocity $v = \omega/k$ at which a propagating mode in one of the layers becomes evanescent. For propagation at angle $\gamma = 90^0$ this occurs when

$v = c_1$ and when $v = c_3$ and the slopes of the two ghost lines are equal to these two values. The ghost lines are associated with long plateau regions of the dispersion curves in which the phase velocity $v = \omega/k$ is virtually constant at a value close to but slightly higher than the ghost wave speed (c_1 *or* c_3).

The second group of results showed plots of the group velocity $c_g = d\omega/dk$ associated with some of the dispersion curves, as a function of wave number k. It is the group velocity which determines the speed of propagation of a pulse and it is shown in the report that at long times the pulses in general decay as $t^{-1/2}$. At local maxima and minima of the group velocity however, the rate of decay of the pulse is $t^{-1/3}$ and it is these wavefront pulses which will therefore persist and dominate the solution at large times and distances. The plots of group velocity show that the plateau regions of the dispersion curves, which are associated with the ghost lines, correspond to long regions of almost constant values of group velocity which are slightly below the associated ghost wave speed (c_1 or c_3). These plateaux occur at local maxima or minima of the group velocity curves and they therefore give rise to the dominant motion at large times. Since these plateau regions appear in the higher harmonics of the dispersion equation they give rise to contributions which are not exhibited by the solutions obtained from the fundamental mode alone nor from approximate plate theories which are designed to reproduce the fundamental mode.

The third group of results showed displacements and stresses at the top and bottom surface of the plate for propagation at the angle $\gamma = 60^0$. These results consisted of graphs showing the variation of both normal and tangential displacements as functions of distance from the impact line at a number of different times. The graphs clearly show the dispersion of the pulse as it propagates. Also included were graphs showing the contributions to the displacement arising from the fundamental modes of symmetric and antisymmetric motion These clearly show that the fundamental mode alone is by no means sufficient to describe the motion and that it is necessary to include the effects of the higher harmonics. Solutions presented using a total of ten modes on the other hand are shown to agree well with the full results obtained using eighteen modes and this leads to the conclusion that the number of modes which were employed should be sufficient to represent adequately the nature of the transient motion.

To sum up, the work carried out under Grant # AFOSR-86-0330 clearly demonstrated that plate bending theories are not suitable to evaluate the transient response of fibre composite laminates to impulsive events. Whilst these theories may be adequate for the determination of vibration modes associated with wavelengths that are large compared with plate thickness, they fail to describe short wavelength high frequency motion that arises in high velocity impact problems. At the same time, the initial results derived under the grant showed that the methods developed have the capacity to yield detailed information concerning the displacement and stress variations in the laminate.

4(b) First Interim Scientific Report on Grant # AFOSR-88-0353, July 1989

This report consisted of two parts, one dealing with further results relating to an upper surface line load impulse acting on the four-ply plate and the other presenting initial results on the response of a six-ply plate and of an eight-ply plate to a line load impulse on the upper surface. The six-ply and eight-ply plates consist of symmetric lay-ups which, in standard notation are written $(-60^0/60^0/0^0)_s$ and $(90^0/-45^0/45^0/0^0)$, respectively. Here, the angles refer to the fibre direction in the ply relative to some reference direction, the suffix s denotes the plate is symmetric about its mid-surface and the entries within the bracket start with the outermost ply on the left and end with the innermost ply on the right. Throughout the first interim report, the material of each ply has been assumed to satisfy the constraint of inextensibility along the fibre direction.

The results presented in the first part relate to line loads acting at angles $\gamma = 0^0, 30^0, 45^0, 60^0$ and 90^0 relative to the fibre direction in the outer layer of the four-ply plate. These results take the form of graphs, each graph consisting of a set of 5, 4 or 3 curves. Each curve shows the variation of one of the stress components as a function of distance parallel to the plate and normal to the impulse line at a fixed time after impact. The 5 curves in a graph give the variation of one stress component at the top surface, the upper interface, the mid-plane, the lower interface and the bottom surface. Where the particular stress component vanishes at the top and bottom surface because of the boundary conditions, the corresponding graph consists of 3 curves which display the component at the two

interfaces and at the mid-plane. Results are given at two different times. One corresponds to the time taken for the fastest wave to travel through a distance of ten plate thicknesses and the other to the time taken for this wave to travel a distance of 50 plate thicknesses. Typical of these results are the sets of curves shown in Figures 3 and 4 which display the in-plane stress component t_{22} at angles $\gamma = 30^0$ and $\gamma = 60^0$. Each figure consists of 4 curves showing the variation of this stress component at the top surface, the upper interface, the lower interface and the bottom surface respectively. The most striking feature of these results is the large amplitude stress to be seen at the upper surface in Figure 3 whereas no such phenomenon is to be seen in Figure 4. This large amplitude component has travelled a distance corresponding to propagation at the speed of a Rayleigh type surface wave. The presence and absence of the surface wave is in agreement with earlier results of Baylis and Green [24]. These show that there exist a range of values of the propagation angle γ, for which the short-wave limiting speed of the fundamental mode of both symmetric and antisymmetric motion is the speed of the Rayleigh type surface wave on the outer layer whereas for values of γ outside this range the short wave limiting speeds of these two modes is the speed of the quasi-shear wave in the core. For waves propagating at angle $\gamma = 30^0$ to the core fibre direction, the stiffening effect of the fibre is greater in the core than in the outer layers, whereas the opposite holds for $\gamma = 60^0$. Since it is the outer layers which have the more significant effect in a bending deformation, it is to be expected that the stiffening in the outer layers at $\gamma = 60^0$ will give rise to higher shearing and lower bending stresses at this angle of propagation than is the case for propagation at $\gamma = 30^0$. Figures 3 and 4 do in fact support this expectation with respect to the bending stresses, since it is evident that the bending stresses shown in Figure 3 are greater than those in Figure 4. Plots of the shearing stress components t_{23} are presented in Figures 5 and 6 for propagation at $\gamma = 30^0$ and $\gamma = 60^0$ respectively. Each of these figures consists of 5 curves. The existence of the non-zero shear stress components t_{23} at the upper and lower surfaces of the plates is a violation of the physical boundary condition which requires that this component of stress should be zero. The presence of the non-zero values arises because of the constraint of inextensibility which gives rise to the possibility of a discontinuity in shear stress parallel to the fibre direction. It is explained in the report that these discontinuities

are to be regarded as narrow boundary layers, in which the shear stress varies rapidly from zero at the surface to the non-zero values which are derived from the inextensibility condition at a level within the material close to the surface. The results presented in Figure 5 and 6 when interpreted in this way therefore give a measure of the level of shearing within the outer plies in regions close to the surfaces as well as giving the values at the interfaces and at the mid-plane. From these Figures it is evident that the shear stress level at $\gamma = 60^0$ is much higher than that at $\gamma = 30^0$, which is again consistent with the expectation outlined above.

The second part of the first interim report dealt with preliminary results for the six-ply and the eight-ply plate. These results showed the variation of upper and lower surface displacements at two different instants of time for a set of different line loads which initiate waves travelling at angles $\gamma = 0^0$, 30^0, 45^0, 60^0 and 90^0 relative to the core fibre direction. The most significant feature of these initial results was the indication of the existence of surface waves at angles of propagation for which the dispersion curves do *not* asymptote the speed of the surface wave in the short-wavelength limit. This phenomenon has been subsequently investigated in detail and the results are reported in the papers by Green [25], [26].

4(c) Second Interim Scientific Report on Grant # AFOSR-88-0353, October 1990

This consisted of three parts. Part 1 dealt with the four-ply inextensible laminate and consisted of a detailed investigation of the penetration of the transient stresses through the layers. Part 2 was devoted to more detailed solutions for the inextensible six-ply and eight-ply plates and Part 3 consisted of the first results for a four-ply plate in which the material was *not* subject to the inextensibility constraint.

It has previously been pointed out that the dominant contributions to the solution at large times comes from the wave fronts which are associated with local maxima and minima of the group velocity. These occur on each branch of the dispersion curves and the relative contributions from each branch are determined by the values of the residues according to equation (21). It is evident from equation (20) that the value of the residue is a function of depth through the plate (x_3) and Part 1 of the second interim report is concerned with examining the nature of this

variation and with the relation of the residues to the stationary values of the group velocity. Figures 7 and 8 are reproduced from that report and each consists of three groups of curves. Figures 7(a) and 8(a) show the phase velocity $v = \omega/k$ and the group velocity $c_g = d\omega/dk$ for the fifth mode of anti-symmetric motion at angles $\gamma = 30^0$ and $\gamma = 60^0$ respectively. In both figures the group velocity exhibits one or more local maxima and minima and both show a long plateau region of the group velocity in the region $12.5 < kh < 16$. Figures 7(b) and 8(b) show plots of the residues associated with the shear stress component t_{23} at 3 levels in the plate. In each Figure the upper curve relates to the top surface, the second and third curve relate to the stress immediately above and immediately below the upper interface and the bottom curve relates to the mid-plane. In each case curves 2, 3 and 4 have been displaced downwards for clarity and the zero levels occur at the values -3, -6 and -9 respectively. There is a very clear distinction between the residues shown in Figure 7(b) and those in Figure 8(b). In Figure 7(b), the upper curve shows contributions to the residue arising at the local minima of the group velocity (including the extended constant portion beyond $kh \approx 16$) with no residue contribution associated with the plateau region at the local maximum. In Figure 8(b) on the other hand, the main contribution to the residue is associated with the local maximum of the plateau region and there is here no contribution associated with the approximately constant group velocity which extends beyond $kh \approx 16$.

Figures 7(c) and 8(c) show plots of the stress contributions as functions of distance from the impact locations which have been calculated using the residues shown in 7(b) and 8(b) respectively. In each of these figures the zero points of curves 2, 3 and 4 have been displaced downwards for clarity to the values -5.0, -10.0 and -12.5 respectively. The two top curves in each figure relate to the shear stress component of the fifth harmonic of antisymmetric motion at the top and bottom of the upper layer whilst the bottom two curves give the corresponding stress at the top and bottom of the lower layer in the top half of the laminate. A detailed discussion of these results is presented in the report.

Part 2 of the second interim report shows the variation of normal displacement as a function of distance from the impulse line at a fixed instant of time for both the six-ply and eight-ply plates of inextensible material. Results are presented for a range of orientations of the line load which correspond to waves

propagating at angles 0^0, 30^0, 45^0, 60^0 and 90^0 relative to the core fibre direction. These results show plots of the displacement at the top and bottom surfaces of the plates and at a number of the internal interfaces between the plies. They show the stiffening effect of the increased number of layers and also demonstrate the way in which the increasing number of layers reduce the penetration of high frequency motion through the plate.

The third part of this interim report contained the first set of results obtained using the unconstrained model for the fibre composite material. The technique was developed by E. R. Green [22] as a modification of a method employed by Mal [23] to study the response to time harmonic surface loads. The results showed plots of the normal displacement of the top and bottom surfaces of the four-ply laminates as a function of distance from the impact line at a fixed time. These plots show a basic long wavelength sinusoidal displacement extending outwards from the impact position and on this basic disturbance is superimposed a short wavelength displacement whose position is consistent with disturbances travelling at speeds approximating those of quasi-shear waves in the various layers of material. Results for the angle of propagation $\gamma = 30^0$ show the existence of a surface wave disturbance on the upper surface of the plate with no trace on the lower surface whereas for disturbances propagating at $\gamma = 60^0$ no such surface wave is apparent. Figure 9 shows a comparison of the top surface displacement for $\gamma = 30^0$ in the extensible model (9(a)) and in the inextensible model (9(b)). The basic disturbance of the latter consists of a downward step in displacement which has travelled the finite distance associated with the plate speed for the long wavelength limit of the inextensible model. Whilst the basic disturbance in the two models is significantly different, it is clear from Figure 9 that the short wavelength motion which is superimposed on the basic disturbance is very similar in the two models. This is a reflection of the fact previously noted that the inextensible model gives good agreement with the extensible except in the long wavelength limit. Since it is the displacement gradient which plays the significant role in the determination of the stresses, the short wavelength displacements are therefore the ones which make the substantial contribution to the stress state and in this respect the two models will yield very similar results.

4(d) Results For the Period 1st October 1990 - 30th September 1991

The results obtained during the final period of the grant fall into two sets. The first set relates to the four-ply plate, using the extensible material model and it is a continuation of the work reported in Part 3 of the second interim report. This work has been carried out by Dr. E. Rhian Green at Leicester University and whilst it has not been financed as part of the research grant, the results are included here since they form an integral part of the overall study. The second set of results are are those for a six-ply plate, again using the extensible material model. This second set of results constitutes the new development carried out in the final year of the grant. Here the plate geometry is a crossply layup having the $(0^0/90^0/0^0)_S$ configuration and the method employed follows closely that developed by E. R. Green [22].

Figures 10 - 25, constitute the first set of results and are relevant to the crossply four layer symmetric plate configurations. Of these, the first four figures (Figures 10 - 13) all show a set of five curves which display the variation of the normal displacement at the top surface, the upper interface, the mid-plane, the lower interface and at the bottom surface of the plate. Each curve in each of the four figures shows the variation of normal displacement with distance from the impact line along the direction of travel of the wave and at the fixed non-dimensional time $T = 200$, where $T = c_1 t/h$. The four figures relate to different orientations γ of the line load relative to the fibre direction in the outer layers. Figures 10 and 11 are for $\gamma = 0^0$ and $\gamma = 30^0$ respectively and both show clearly the existence of a surface wave on the top surface which has virtually vanished at the upper interface. No such surface wave exists in Figures 12 and 13, which correspond to $\gamma = 60^0$ and $\gamma = 90^0$ respectively. The upper and lower surface normal displacements for the inextensible model at $T = 200$ are to be found in the paper by Green and Baylis [27] when Figures 6, 7, 9 and 10 relate to $\gamma = 0^0, 30^0, 60^0$ and 90^0 respectively. It may be seen from these two sets of figures that the basic underlying motion is a long wavelength sinusoid for the extensible model and a downward step displacement for the inextensible model. Each basic motion has a superimposed shorter wavelength oscillation and a comparison of the two sets of figures shows that this superimposed motion is very similar for the corresponding values of γ in the two models. The conclusion is that the inextensible results should provide an

accurate approximation to the behaviour except in the long wavelength limit.

Examples of the stress variations through the thickness in the four-ply plate are to be seen in Figures 14 - 17. Each of these figures consists of three curves which show the variation of stress with distance from the impact line at the upper interface, the mid-plane and lower interface. Figures 14 and 15 relate to the normal stress component t_{33} for line loads at orientation $\gamma = 30^0$ and $\gamma = 60^0$ respectively. Figures 16 and 17 show the shear stress component t^*_{13} associated with the propagation direction and defined by

$$t^*_{13} = t_{13}\ cos\gamma + t_{23}\ sin\gamma\ ,$$

with Figure 16 relating to $\gamma = 30^0$ and Figure 17 to $\gamma = 60^0$. Both stress components t_{33} and t^*_{13} are zero at the outer surfaces of the plate. These graphs clearly show the surface wave effect at the upper interface for $\gamma = 30^0$ (Figures 14 and 16) and its absence for $\gamma = 60^0$ (Figures 15 and 17). The overall magnitudes of the two stresses are higher at $\gamma = 30^0$ than at $\gamma = 60^0$ but the spatial extent of the disturbance is generally bigger at $\gamma = 60^0$ than at $\gamma = 30^0$. This latter result thus implies that at any fixed point the relatively high stress level would persist for a longer time for a line load at $\gamma = 60^0$ than for a load at $\gamma = 30^0$. It is of interest to compare the results presented in Figures 16 and 17 with the corresponding solutions derived for the inextensible four-ply plate, which were reported in the first interim report (Figures 14 and 16) and which are reproduced here as Figures 18 and 19. Taking into account the fact that the two sets of results are plotted on different scales it is clear that there is a good correlation between the extensible and inextensible models.

The results presented heretofore have all involved the response to a line load represented by a Dirac delta function in time. It has already been remarked that whilst such an impulse is not a practical reality, the solution derived from it may be employed to obtain results for any other time history of the line load, by convolution. This procedure has been carried out by E. R. Green [28], [29], [30], who has derived the solutions for square pulses, half sine wave pulses and full sine wave pulses each of three different durations. Figures 20 and 21 show the plate response to square pulses of three different durations. The curves in Figure 20 show the upper surface normal displacement for pulses of duration $T = 0.1$, $T = 1.0$

and $T = 10.0$ respectively and for $\gamma = 30^0$. It is clear from these curves that the effect of increasing the duration of the pulse is to reduce the amplitude of the high frequency disturbance in comparison with the amplitude of the underlying basic sinusoidal motion, associated with the long wavelength beam bending behaviour. Shown in Figure 21 is the upper interface normal stress component t_{33} associated with the same three pulses as in Figure 20. Attention is drawn to the fact that the lowest of these three curves is plotted on a vertical scale which differs from the other two. Here also it is clear that the comparative amplitudes of the high frequency stresses are drastically reduced by increasing the pulse length. It is noted however that the contribution of the basic bending disturbance to the overall stress is negligible in comparison with the contributions of the high frequency components. This is evident in particular from the bottom curve in Figure 21 which shows rapid stress variation in the region $100 < x/h < 110$ whereas the corresponding displacement curve in Figure 20 shows virtually no trace of a high frequency component.

Additionally to the developments outlined above, the response of the four-ply plate to an internal delta function line load acting at the ply interfaces or on the mid-plane have also been obtained and reported in references [31] and [32]. Figures 22 - 25 are reproduced from these publications. Each figure consists of a set of five curves showing the normal displacement at time $T = 200$ on the two surfaces, the interfaces and the mid-plane. Figures 22 and 23 correspond to propagation angles $\gamma = 30^0$ and $\gamma = 60^0$ respectively and they relate to the delta function line load acting at the upper interface. For Figures 24 and 25 the line load acts at the mid-plane and initiates waves propagating at $\gamma = 30^0$ and $\gamma = 60^0$ respectively. These four figures are to be compared to Figures 11 and 12 which show the corresponding results for the upper surface line load. A particular point to note in this comparison is that curve (ii) of Figure 11 is identical with curve (i) of Figure 22, curve (iv) of Figure 11 is identical with curve (v) of Figure 22, curve (iii) of Figure 11 is identical with curve (i) of Figure 24 and curve (iii) of Figure 22 is identical with curve (ii) of Figure 24. Similar identities hold for the corresponding curves in Figures 12, 23 and 25. These phenomena are all manifestations of a reciprocal property of the Green's function solutions, which is discussed in detail in Green and Green [33].

The second set of results relates to the six-ply $(0^0/90^0/0^0)_S$ plate and are presented in Figures 26 - 29 . Of these, the first two, Figures 26 and 27, each consist of seven curves. Each curve shows the variation of normal displacement with distance from the impact line, at a fixed instant of time $T = 20$ in Figure 26 and $T = 40$ in Figure 27. The seven curves relate to the displacement at the top and bottom surface, the four interfaces and the mid-plane The line load is chosen to be parallel to the fibre direction of the outer ply and initiates a disturbance travelling in the plate at angle $\gamma = 90^0$ to the core fibre direction. Both Figures 26 and 27 show evidence of a surface wave disturbance travelling on the top surface of the plate and which persists to some extent on the upper interface. This surface wave phenomenon is not unexpected since the angle of propagation relative to the fibre direction in the outer layer is also 90^0 and the limiting speed of the fundamental mode of harmonic waves in the plate will then be that of the Rayleigh surface waves in the direction orthogonal to the fibres. The position of this high amplitude disturbance in Figures 26 and 27 corresponds to a speed of propagation $v/c_1 \approx 0.42$ which is in good agreement with this Rayleigh wave speed.

Figures 28 and 29 show displacement plots at time $T = 40$ in the four-ply plate. Each figure consists of five curves which show the displacements at the two surfaces, the two interfaces and the mid-plane. Of these, Figure 28 is for $\gamma = 0^0$, which corresponds to propagation along the fibre direction in the core and at right angles to the fibre direction in the outer layers. Figure 29 relates to $\gamma = 90^0$, for which the disturbance is parallel to the fibre direction in the outer layers. These two figures have been included for the purpose of comparison with Figure 27 and it is evident that the six-ply results presented in Figure 27 agree much more closely with the four-ply results in Figure 28 than with those in Figure 29. It would thus seem that the dominant characteristics of the motion are determined by the orientation of the line load relative to the fibre direction in the outer layers. Nevertheless, the presence of a more significant short wavelength (high frequency) content in Figure 27 than in Figure 28, mirrors the fact that the overall depth of the laminate does also contribute to the nature of the disturbance.

The final two figures (Figures 30 and 31) show plots of the stress variation at different levels in the six-ply plate at time $T = 40$. Each figure consists of five curves showing the stresses at the four interfaces and at the mid-plane. The curves

in Figure 30 relate to the normal stress component t_{33} whilst those in Figure 31 relate to the shear stress component t_{23} parallel to the direction of propagation. Both these stress components vanish at the outer surfaces of the plate in virtue of the boundary conditions. It is these stress components which are expected to determine whether or not delamination will occur. In the configuration which is examined here, the highest stress levels obviously occur at the uppermost interface, which is therefore the region most prone to delamination. Additionally, the presence of a region of a rapidly varying stress, albeit at a much lower magnitude, is evident at the lowest interface. The possibility exists of these low level rapid stress variations producing some weakening of the interface bond by cumulative fatigue damage.

5. DISCUSSION AND CONCLUSIONS

Stress wave propagation in elastic bodies is a highly complex phenomenon. In any elastic material there can exist in general three distinct waves which will travel in a specified direction at a point. For isotropic materials two of these waves have the same speed and the associated displacement is transverse to the propagation direction whilst the displacement of the remaining wave is polarised along the direction of propagation. For anisotropic materials, the three speeds are generally distinct, they vary with the direction of propagation and there is no simple relation between the direction of propagation and the polarisation vectors. Any one of these waves when incident on the boundary of the elastic body will give rise to three reflected waves (one of each type) travelling back into the body. If the boundary is the interface between two different elastic materials, then the incident wave will, in addition, generate three transmitted waves propagating away from the interface into the adjacent material. Each of these reflected and transmitted waves will in turn generate th ee reflected waves on reaching any boundary, together with three transmitted waves if the boundary forms an interface between two materials.

From these considerations it is evident that, in a multilayered plate, the initiation of a single wave emanating from one point sets up a multiplicity of disturbances associated with reflection and transmission at the interfaces and reflection at the outer boundaries. Even in a single plate of isotropic elastic material, in which there are no interfaces, the generation of two reflected waves by

every wave incident on each of the two boundaries of the plate leads to a rapid escalation of the wave count deriving from a single initiating disturbance. The cumulative effect of these multiple reflected waves gives rise to the waveguide modes. These consist of harmonic waves, travelling parallel to the plane of the plate and with speed of propagation which varies with frequency. The relation between the wave speed and the frequency in a plate of isotropic elastic material is governed by the Rayleigh/Lamb dispersion equation. This equation separates into two factors, one associated with a symmetric motion of the plate and the other with antisymmetric motion. Each factor possesses an infinity of branches, corresponding to the different modes of wave motion.

The displacements and stresses associated with the Rayleigh/Lamb modes vary with distance through the plate, in a manner which depends on the particular branch (mode) and on the frequency of the harmonic motion. In particular, for the first branch (fundamental mode) of antisymmetric motion, the in-plane displacements vary linearly with distance from the middle surface whilst the normal displacement becomes uniform through the thickness, in the limit as the frequency tends to zero (long wavelength limit). This is the form of displacement which is assumed in the simple (Euler-Bernoulli) theory of plate bending and the results derived using that theory are valid when the wavelength of the deformation is large in comparison with the plate thickness. As the frequency increases from zero, the displacements associated with the fundamental mode of antisymmetric motion deviate from those employed in the Euler-Bernoulli theory becoming more non-uniform through the thickness. Increasing frequency is associated with decreasing wavelength and, in the limit as the wavelength tends to zero, the displacements take a form which decreases exponentially with distance into the plate from each of the two faces. Displacements having this exponential decay are associated with a Rayleigh surface wave travelling in a half space of the material and the limiting speed of short waves in the fundamental mode agrees with the Rayleigh wave speed. All modes higher than the fundamental exhibit a cut-off frequency associated with the long wavelength limit. For these, the displacements are non-uniform through the thickness, having a number of nodal points, the number increasing with the order of the mode.

Weaver and Pao [13] have shown that the transform technique, which has

been employed here in order to solve the problem of impact loading, is equivalent to expressing the solution as a superposition of the modes of the Rayleigh Lamb equation. The magnitude of the contributions from the different modes depends on the nature of the time history and on the spatial distribution of the impact load. However, it is clear that the stress variation through the plate thickness, which arises from this superposition will be highly nonlinear and that an attempt to represent this variation by using simple plate bending theory must be inadequate. Whilst the considerations of Weaver and Pao relate to a single plate of isotropic elastic material, the same conclusion can be drawn regarding the multi-ply laminates of anisotropic elastic material which have been treated in this project.

The work carried out in this project has demonstrated the application of the full three dimensional equations of anisotropic elasticity to the study of transient wave motion in laminated plates. It has been shown that an impulsive line load acting on the upper surface of the laminate will generate dynamic stresses which vary significantly with depth. This depth variation cannot be reproduced by using theories such as classical laminate theories which are based on a simple plate bending assumption, since these by their nature involve a built-in linear stress variation through each of the plies.

Analytical solutions have been obtained for the double transforms of displacements and stresses for 4-ply, 6-ply and 8-ply laminates using a simplified model in which the material is treated as inextensible in the fibre direction. The analysis was subsequently extended and solutions obtained for 4-ply and 6-ply laminates using a more realistic model which does *not* assume inextensibility of the materials in the fibre direction. These analytic solutions are exact within the framework of the theory which treats the fibre composite plies as transversely isotropic homogeneous elastic continua. Approximations are introduced only in the process of numerical inversion of these transform solutions. These approximations arise in two ways. Firstly, by restricting the summation over the infinite number of modes to a finite sum and secondly, by replacing integration over an infinite range of wavenumbers by integration over a finite range. In the second approximation the finite range of integration is chosen so as to be consistent with the range of validity of the homogeneous continuum assumption For wavenumbers outside this range the wavelengths are of the same order as the fibre diameters and inter-fibre spacing

or less, and the homogeneous continuum assumption is not valid. At such wavelengths there will be multiple scattering and diffraction which results in a loss of coherence and leads to these waves being, in effect, damped out. As regards the first approximation, results obtained in the preliminary investigation (Grant # AFOSR86-0330) showed that the choice of ten modes for each of the symmetric and the antisymmetric disturbances is more than adequate to include all the significant contributions arising from the finite range of values of the wave number.

The detailed plots of displacements and stresses which have been obtained in this project constitute a new contribution to the study of impact waves in laminated plates. They have given rise to a total of 15 published papers which have appeared in refereed journals and conference proceedings. These are listed in the Appendix 1. One of the most striking features of the work is concerned with the surface wave phenomenon. In the case of the four-ply plate a surface wave exists for a particular range of angles but not for angles outside this range. This is not the situation for the six-ply and eight-ply plates, where the surface wave appears at all angles of propagation. The explanation of this anomaly is to be found in the behaviour of the dispersion curves associated with the propagation of harmonic waves in the laminate.

It transpires that the surface wave can arise in one of two ways. In the first instance, the limiting short wave speed of the fundamental mode for both symmetric and antisymmetric wave motion is that associated with a Rayleigh type surface wave, travelling at the specified angle in the outer layer. The limiting short wave speed of all other modes is that of the slowest quasi shear wave travelling at the specified angle in the outer layer. The surface wave associated with the impact then arises solely from the fundamental modes of the harmonic motion. In the second instance, the limiting short wave speed of all modes of harmonic motion is less than that of a Rayleigh type surface wave travelling at the specified angle in the material of the outer layer. When this situation pertains, the dispersion curves associated with the higher harmonics exhibit plateau regions on which the phase velocity and the group velocity are approximately constant over a range of values of the wave number. The phase and group velocity associated with each plateau are equal to the speed of the Rayleigh type surface wave in the outer material and the

surface wave arising from the impact is, in this instance, generated by the cumulative contributions from these plateau regions in the summation over the modes. The order of the harmonic on which the plateau region first appears and the range of values of wavenumber over which the plateau extends, are both functions of the overall depth of the plate. In these investigations, the depth is proportional to the total number of plies and, for the range of values of wavenumber over which the integration takes place, the harmonics of the four-ply plate do not exhibit the plateau region whereas those of the six-ply and eight-ply plate do so. A more detailed treatment of the effect is to be found in the paper by Green [26].

Comparison of the detailed results derived using the inextensible material model with those obtained from the more realistic model, which does not assume inextensibility, showed significant differences between the predicted normal displacements in the two cases. This arose out of the difference in the behaviour of the two models in the long wavelength limit. Here the inextensible plate undergoes a shearing deformation whilst the extensible deforms in bending in the classical St. Venant or Euler/Bernoulli mode. Apart from this discrepancy of the underlying deformation mode, the shorter wavelength contributions to the displacement are very similar in the two models. This strong similarity is even more pronounced on comparing the stresses. The underlying long wavelength deformation makes little contribution to the stresses, which in the main arise from the larger strains associated with short wavelength displacements A comparison of the stresses shows that the results derived from the inextensible model yield a very good approximation to those obtained on removing the inextensibility constraint. Since the two sets of results have been obtained using entirely different numerical approaches, the extent of this agreement also serves to give confidence in the accuracy of the numerical procedures.

One of the main reasons for evaluating the transient stresses which arise from impact events is in an attempt to determine the location and extent of any delamination which may occur. A number of different criteria have been proposed in the literature in order to determine whether or not delamination takes place. Amongst these are the maximum tensile normal stress criterion, the maximum shear stress criterion and cumulative damage criteria which involve the time integration of

the tensile normal stress or the time integration of the shear stress. Here it is not intended to examine any of these in detail but it is pertinent to remark that the techniques which have been developed in this project provide the detailed information to enable any of these criteria to be applied in any specified laminate geometry.

On the basis of the contents of this report, the preceding interim reports and the published work listed in Appendix 1, it is claimed that the project has demonstrated the validity of the following conclusions.

1. The three dimensional equations of elasticity, coupled with the appropriate transform techniques and numerical transform inversion are capable of predicting in detail the transient stress state resulting from surface impact on fibre composite laminated plates.
2. The detailed nature of the interfacial stresses varies significantly with both the direction of wave propagation and with depth through the laminate. The nature of this variation is such that it cannot be predicted using methods which adopt the simple engineering mechanics approach to model the deformation.
3. Surface impacts will initiate Rayleigh type surface waves propagating within a specified range of angles on any laminate. Outside this range of angles, the existence of the surface wave depends on the overall laminate depth.
4. The use of a simplified material model, which treats the fibre composite as inextensible in the fibre direction, yields stress levels which are in good agreement with those derived using a more realistic model. The simplified material model affords a substantial reduction in computational effort. To the extent that the material parameters, such as elastic moduli, ply thickness, accuracy of fabrication, are prone to error, the results of the simplified model may well be acceptable.
5. The techniques employed to study surface impacts are equally applicable to the investigation of transients arising from internal events such as delamination or fracture. In particular, these methods have a potential application to the emerging neural network approach to the location of internal faults by acoustic emission.

APPENDIX

LIST OF PUBLICATIONS ARISING FROM THE RESEARCH GRANTS

1. W. A. Green and E. R. Baylis. 'The propagation of impact stress waves in anisotropic fibre reinforced laminates', in Wave Propagation in Structural Composites (edited by A. K. Mal and T.C.T. Ting), AMD-Vol.90 pp.53-68. ASME, New York, 1988.

2. E. R. Baylis and W. A. Green. 'Impact stress waves in fibre reinforced laminated plates', in Proc. 3rd Int. Conf. on Recent Advances in Structural Dynamics (edited by M. Petyt, H. F. Wolfe and C. Mei), Vol. 1 pp.171-183. AFWAL-TR-88-3034, University of Southampton, 1988.

3. W. A. Green and E. R. Baylis. 'The contribution of high-harmonics to transient waves in plates and laminates, Ibid pp.185-197.

4. W. A. Green. 'Stress-wave propagation in a laminated sandwich plate', in Elastic Wave Propagation (edited by M. F. McCarthy and M. A. Hayes), pp.189-194. North-Holland, Amsterdam, 1989.

5. W. A. Green. 'Elastic waves in laminated plates of inextensible material', in Elasticity: mathematical methods and applications (edited by G. Eason and R. W. Ogden), pp.135-164. Ellis Horwood, Chichester, 1990.

6. W. A. Green. 'Transient stress waves in anisotropic laminates', in Elastic Waves and Ultrasonic Nondestructive Evaluation (edited by S.K. Datta, J.D. Achenbach and Y.S. Rajapakse), pp.417-418. North-Holland, Amsterdam, 1990.

7. W. A. Green and E. R. Green. 'Impact stress waves in fibre composite laminates', in Developments in the Science and Technology of Composite Materials (edited by J. Füller, G. Grüninger, K. Schulte, A.R. Bunsell and A. Massiah), pp.993-998. Elsevier Applied Science, London, 1990.

8. W. A. Green and E. Rhian Green. 'Penetration of impact stresses in laminated composite plates', in Impact Response and Elastodynamics of Composites (edited by A.K. Mal and Y.D.S. Rajapakse) AMD-Vol.116, pp.135-152. ASME, New York, 1990.

9. W. Anthony Green. 'Reflection and transmission phenomena for transient stress waves in fiber composite laminates', in Review of Progress in Quantitative Nondestructive Evaluation (edited by D.O. Thompson and D.E. Chimenti), Vol.10B, pp.1407-1414. Plenum Press, New York, 1991.

10. W. A. Green and E. Rhian Green. 'Stress variation due to an impact line load on a four-ply fibre composite plate'. Int. J. Solids & Structures, Vol. 28, pp.567-594, 1991.

11. G. A. Rogerson. 'Dynamic response of an eight-ply composite plate to an impulsive line load'. Mechanics Research Communications, Vol. 18, pp.385-394, 1991.

12. W. A. Green. 'Surface wave propagation in fiber composite laminates', in Review of Progress in Quantitative Nondestructive Evaluation (edited by D. O. Thompson and D. E. Chimenti), Vol. 11. Plenum Press, New York, to appear.

13. G. A. Rogerson. 'Penetration of impact waves in a six-ply fibre composite laminate', to appear in Journal of Sound and Vibration, 1992.

14. W. A. Green, G. A. Rogerson and D. Milosavljevic. 'Transient waves in six-ply and eight-ply fiber composite plates', to appear in Composites Science and Technology, 1992.

15. E. Rhian Green and W. A. Green. 'Reciprocal relations for dynamic Green's functions in fibre composite laminates', to appear in Journal of Mechanics and Physics of Solids, 1992.

REFERENCES

[1] Miklowitz, J. Modern Problems in Elastic Wave Propagation. Wiley, New York, 1978.

[2] Ting, T.C.T. Applied Mechanics Reviews, **33**, pp.1629-1635, 1980.

[3] Pao, Y-M. ASME Jour. App. Mech. **50**, pp.1152-1164, 1983.

[4] Kapania, R.K. and Raciti, S. AIAA Journal, **27**, pp.935-945, 1989.

[5] Chow, T.S. J. Composite Materials, **5**, pp.306-319, 1971.

[6] Moon, F.C. J. Composite Materials, **6**, pp.62-79, 1972.

[7] Sun, C.T. J. Composite Materials, **7**, pp.366-382, 1973.

[8] Liu, G.R., Tani, J., Ohyoshi, T. and Watanabe, K. ASME Jour. of Vibration and Acoustics, pp.230-238, 1991.

[9] Lee, J.D., Du, S. and Liebowitz, M. Computers and Structures, **19**, pp.807-812, 1984.

[10] Wu, M.T. and Springer, G.S. J. Composite Materials, **22**, pp.533-560, 1988.

[11] Miklowitz, J. The Theory of Elastic Waves and Waveguides. North Holland, Amsterdam, 1978.

[12] Ceranoglu, A.N. and Pao, Y.M. ASME Jour. App. Mech., **48**, pp.125-147, 1981.

[13] Weaver, R.L. and Pao, Y.M. ASME Jour. App. Mech., **49**, pp.821-836, 1982.

[14] Vasudevan, N. and Mal. A.K. ASME Jour. App. Mech., **52**, pp.356-362, 1985.

[15] Willis, J.R. and Bedding, R.J. Modern Problems in Elastic Wave Propagation (J. Miklowitz and J.D. Achenbach, Eds.). Wiley, New York, pp.347-371, 1978.

[16] Stone, S.F. and Chatterjee, A.K. Impact Response and Elastodynamics of Composites, (A.K. Mal and Y.D.S. Rajapakse, Eds.). ASME-AMD, **116**, pp.27-50, 1990.

[17] Sachse, W. Elastic Waves and Ultrasonic NDE, (S.K. Datta, J.D.Achenbach and Y.D.S. Rajapakse, Eds.). Elsevier, Amsterdam, pp.285-294, 1990.

[18] Markham, M.F. Composites, **1**, pp.145-149, 1970.

[19] Green, W.A. Quart. J. Mech. Appl. Math. **35**, pp.485-507, 1982.

[20] Baylis, E.R. and Green, W.A. J. Sound Vibr., **110**, pp.1-26, 1986.

[21] Spencer, A.J.M. Deformations of Fibre-reinforced Materials. Oxford, 1972.

[22] Green, E.R. Acta Mech., **86**, pp.153-165, 1991.

[23] Mal, A.K., Wave Motion, **10**, pp.257-266, 1988.

[24] Baylis, E.R. and Green, W.A. J. Sound Vibr., **111**, pp.181-190, 1986.

[25] Green, W.A. Review of Progress in QNDE, **10B** (D.O. Thompson and D.A. Chimenti, Eds.). Plenum Press, New York, pp.1407-1414, 1991.

[26] Green, W.A. Review of Progress in QNDE, **11** (to appear).

[27] Green, W.A. and Baylis, E.R. Wave Propagation in Structural Composites, (T.C.T. Ting and A.K. Mal, Eds.) ASME-AMD, **90**, pp.53-67, 1988.

[28] Green, E.R. Applied Mechanics **4**, (A.C.F. Cocks and A.R.S. Ponter, Eds.). Elsevier, Amsterdam, pp.19-35, 1991.

[29] Green, E.R. Enhancing Analysis Techniques for Composite Materials, (L. Schwer, J.N. Reddy and A.K. Mal, Eds.). ASME-NDE, **10**, pp.9-21, 1991.

[30] Green, E.R. ASME Jour. Appl. Mech. (to appear).

[31] Green, E.R. Review of Progress in QNDE, **10B** (D.O. Thompson and D.A. Chimenti, Eds.). Plenum Press, New York, pp.1399-1406, 1991.

[32] Green, E.R. Review of Progress in QNDE, **11** (to appear).

[33] Green, E.R. and Green, W.A. Journ. Mech. Phys. Solids (to appear).

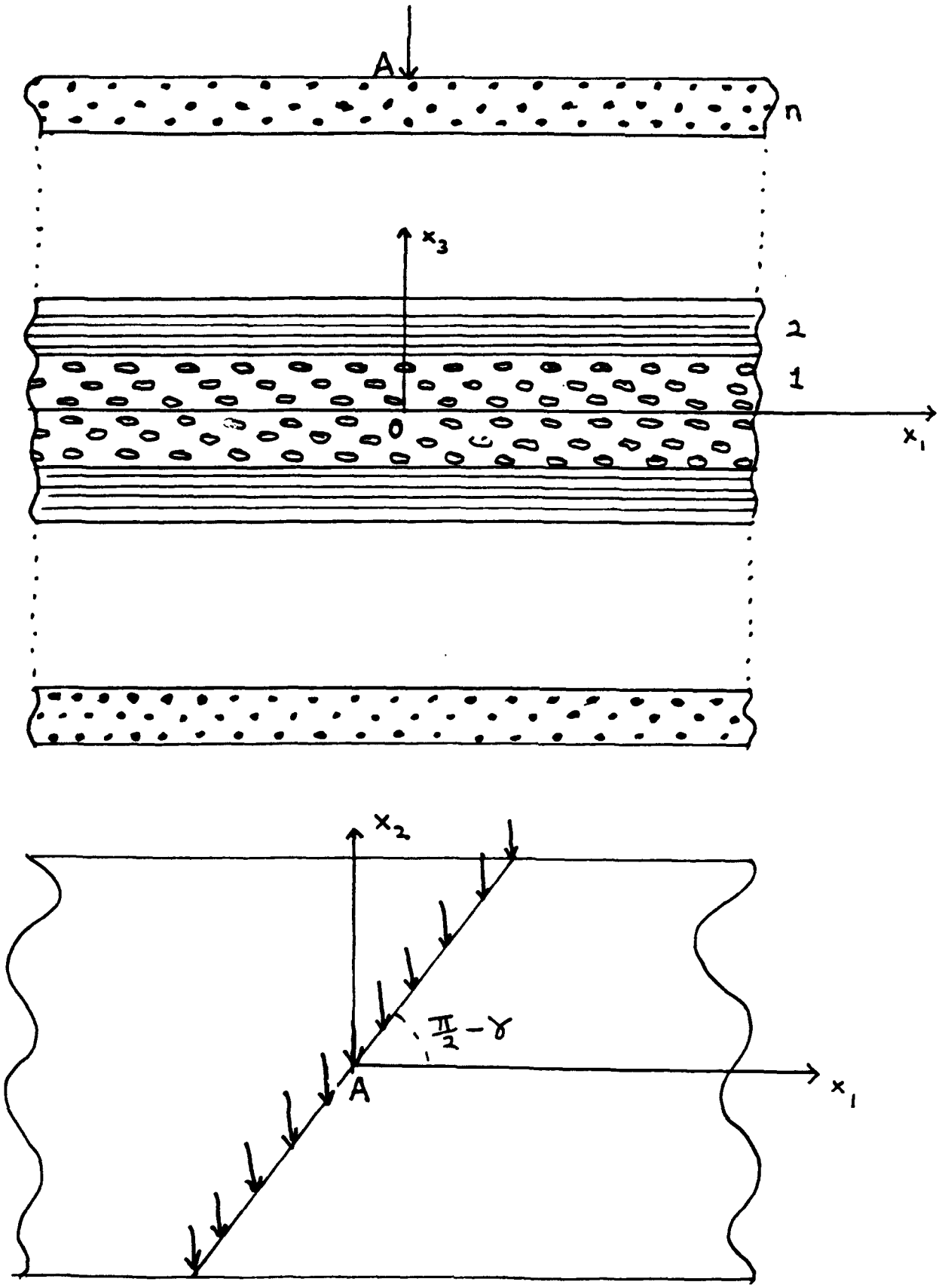

Figure 1 Geometry of $2n$-ply plate and upper surface line loading.

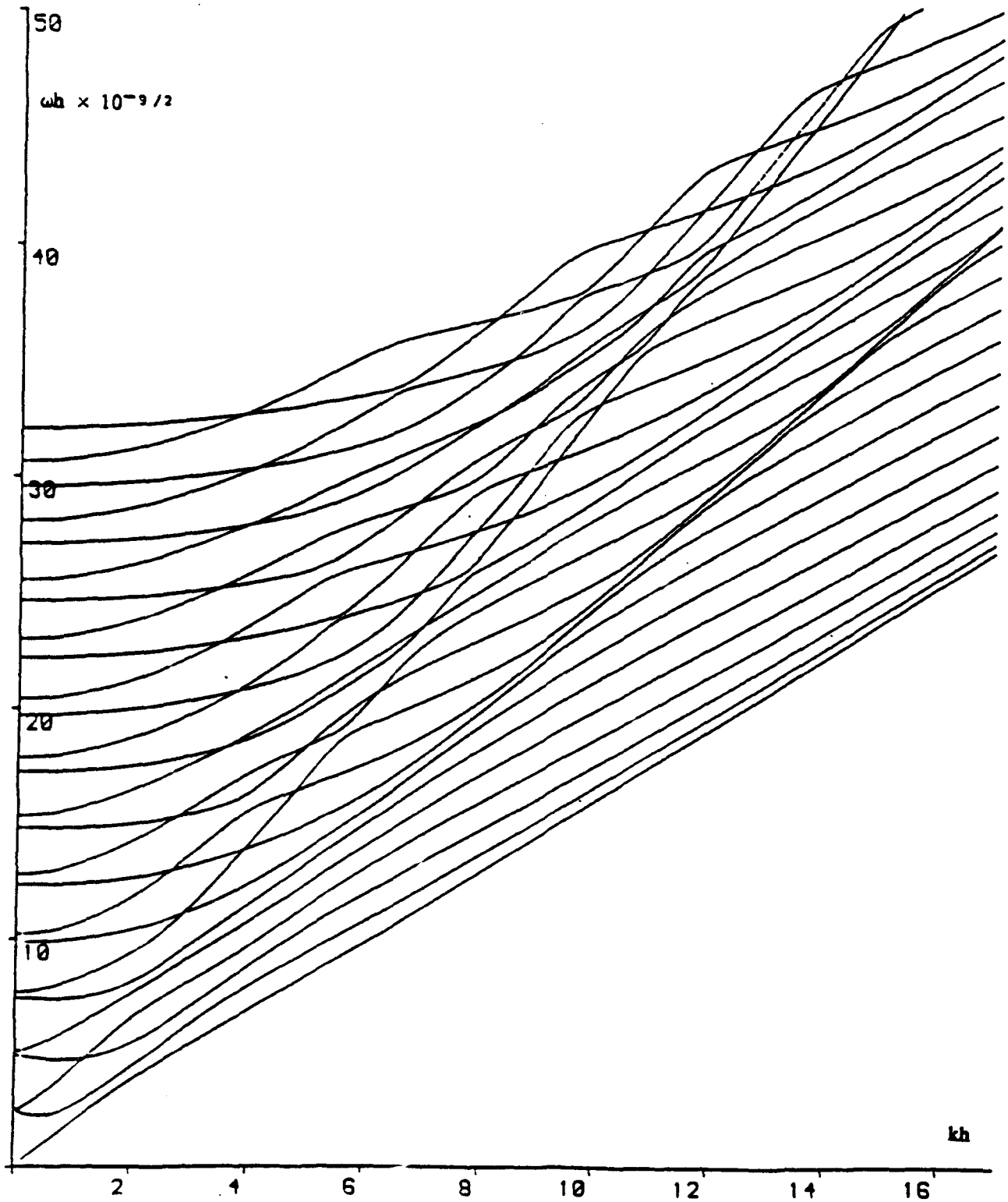

Figure 2 Dispersion curves for first 26 modes of harmonic wave propagation in 4-ply plate. $\gamma = 90°$.

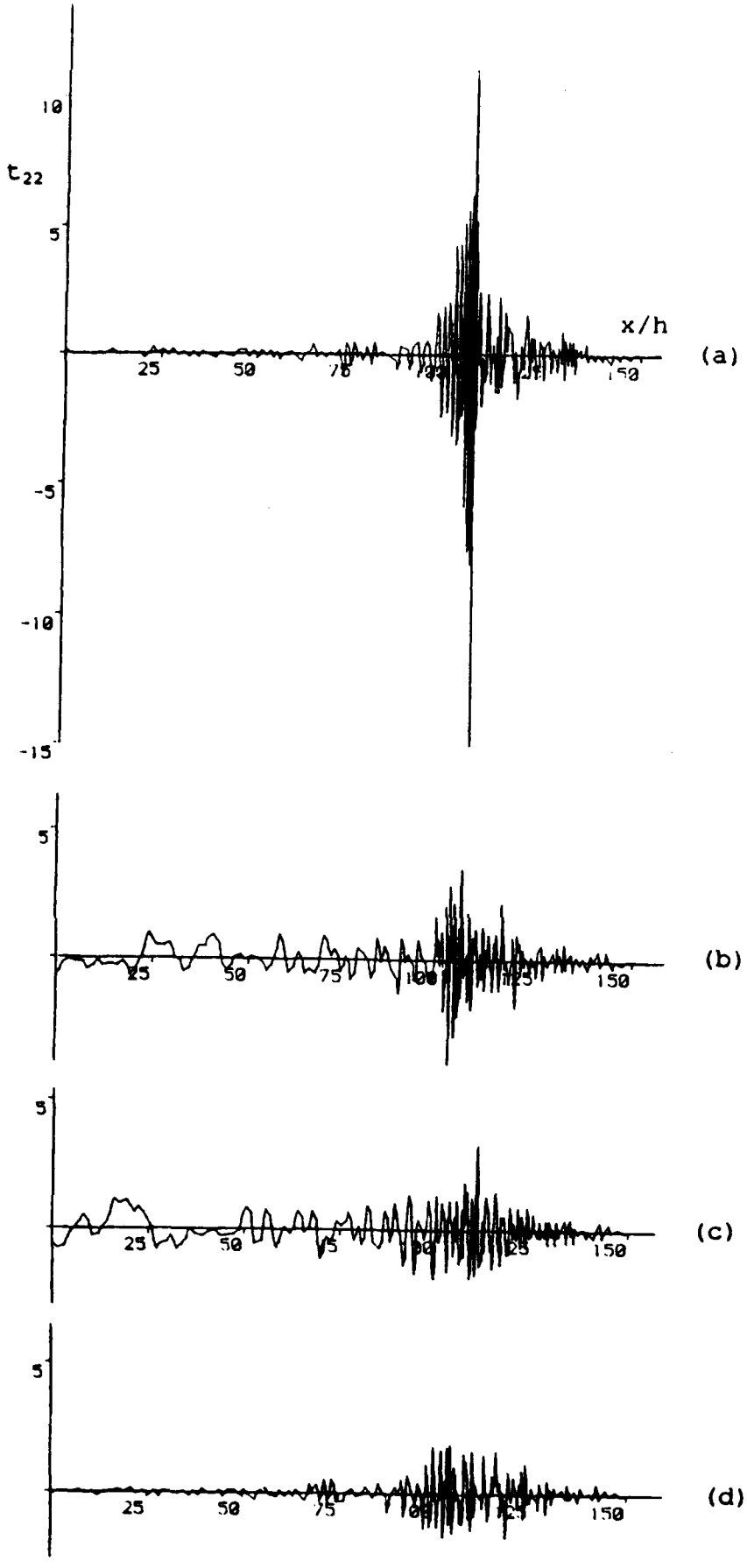

Figure 3 Stress component t_{22} in 4-ply plate at time $t = 200h/c_1$ for $\gamma = 30^0$ at:

(*a*) upper surface (*b*) upper interface

(*c*) lower interface (*d*) lower surface

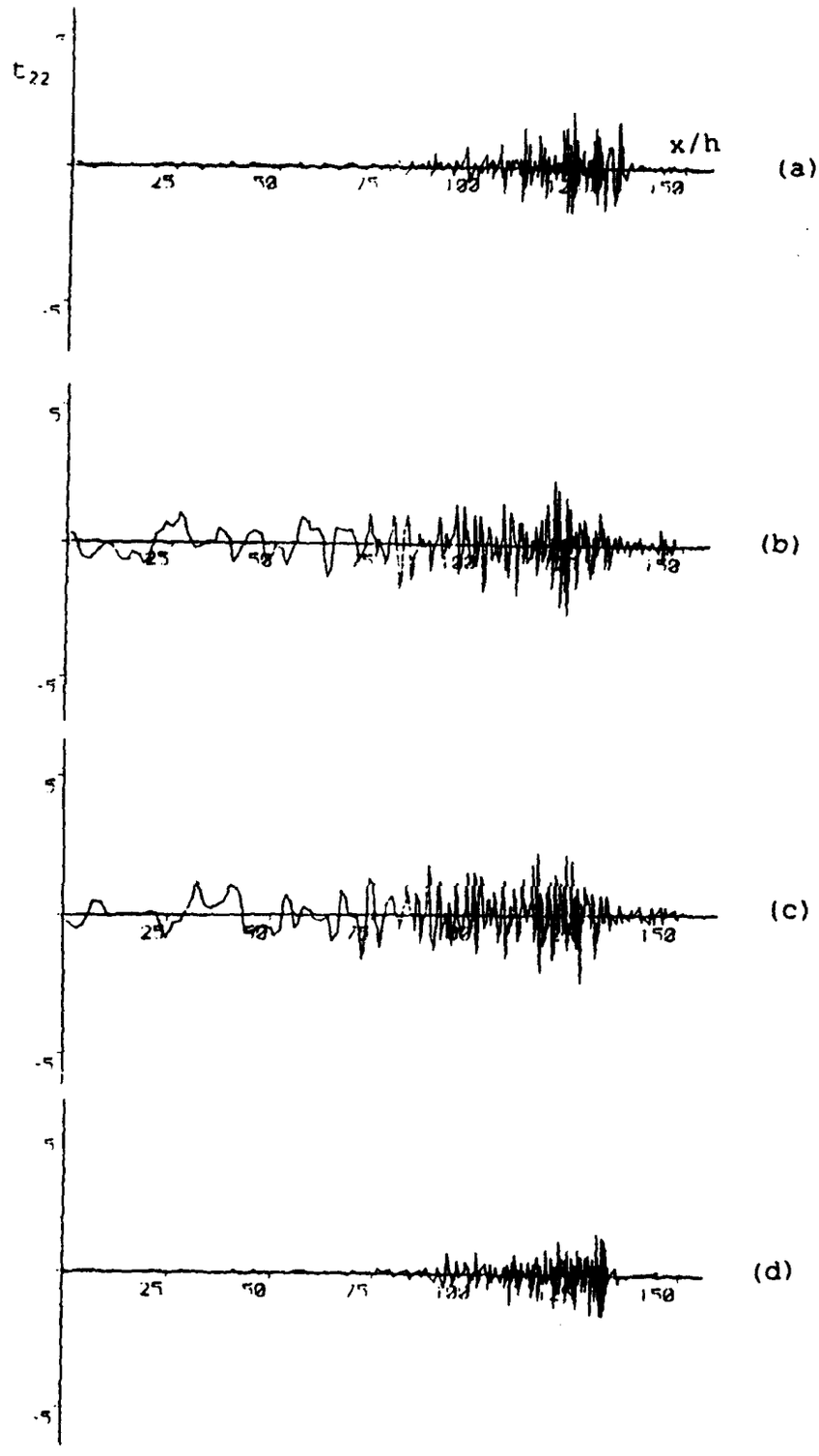

Figure 4 Stress component t_{22} in 4-ply plate at time $t = 200h/c_t$ for $\gamma = 60°$ at:

(*a*) upper surface (*b*) upper interface

(*c*) lower interface (*d*) lower surface

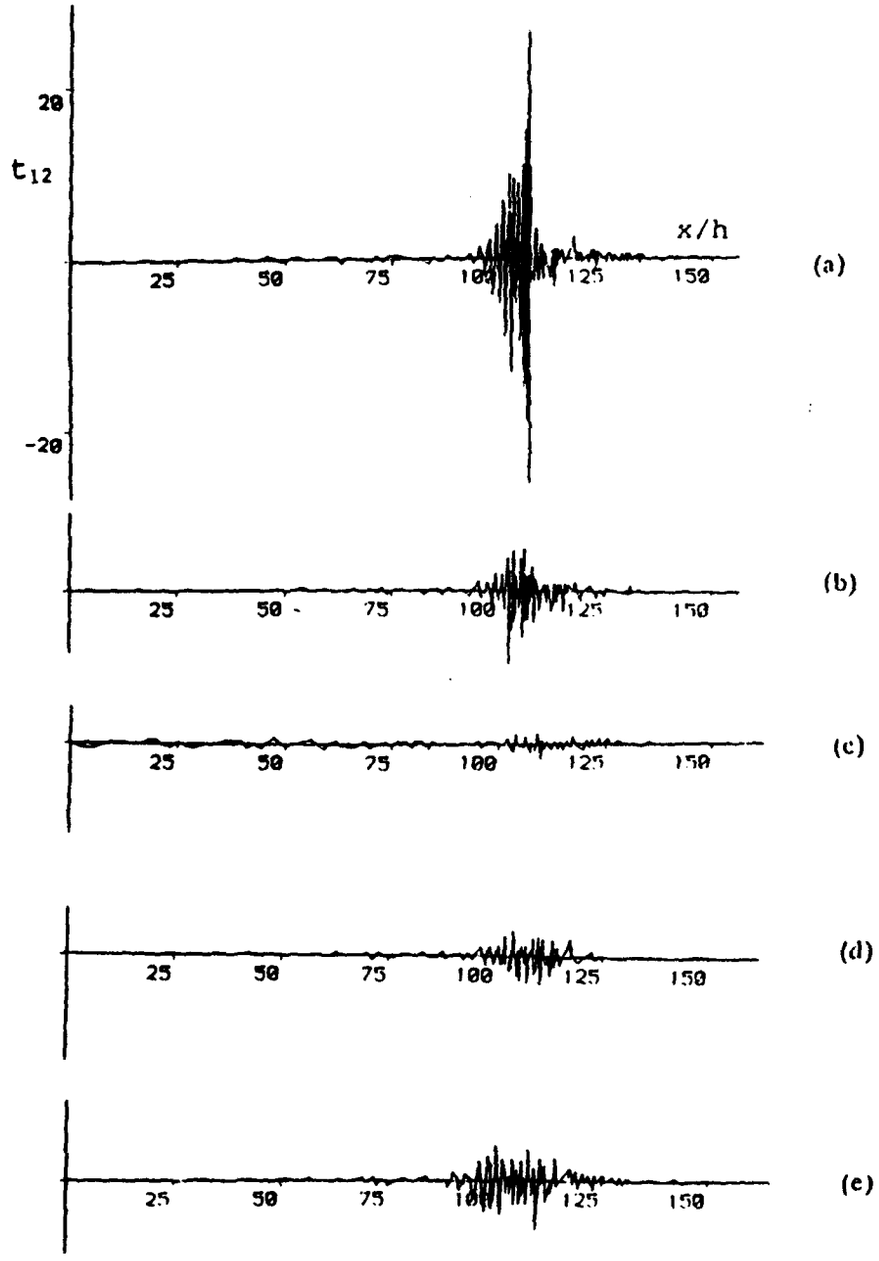

Figure 5 Stress component t_{12} in 4-ply plate at time $t = 200h/c_1$ for $\gamma = 30^0$ at:
(*a*) upper surface (*b*) upper interface (*c*) mid-surface
(*d*) lower interface (*e*) lower surface

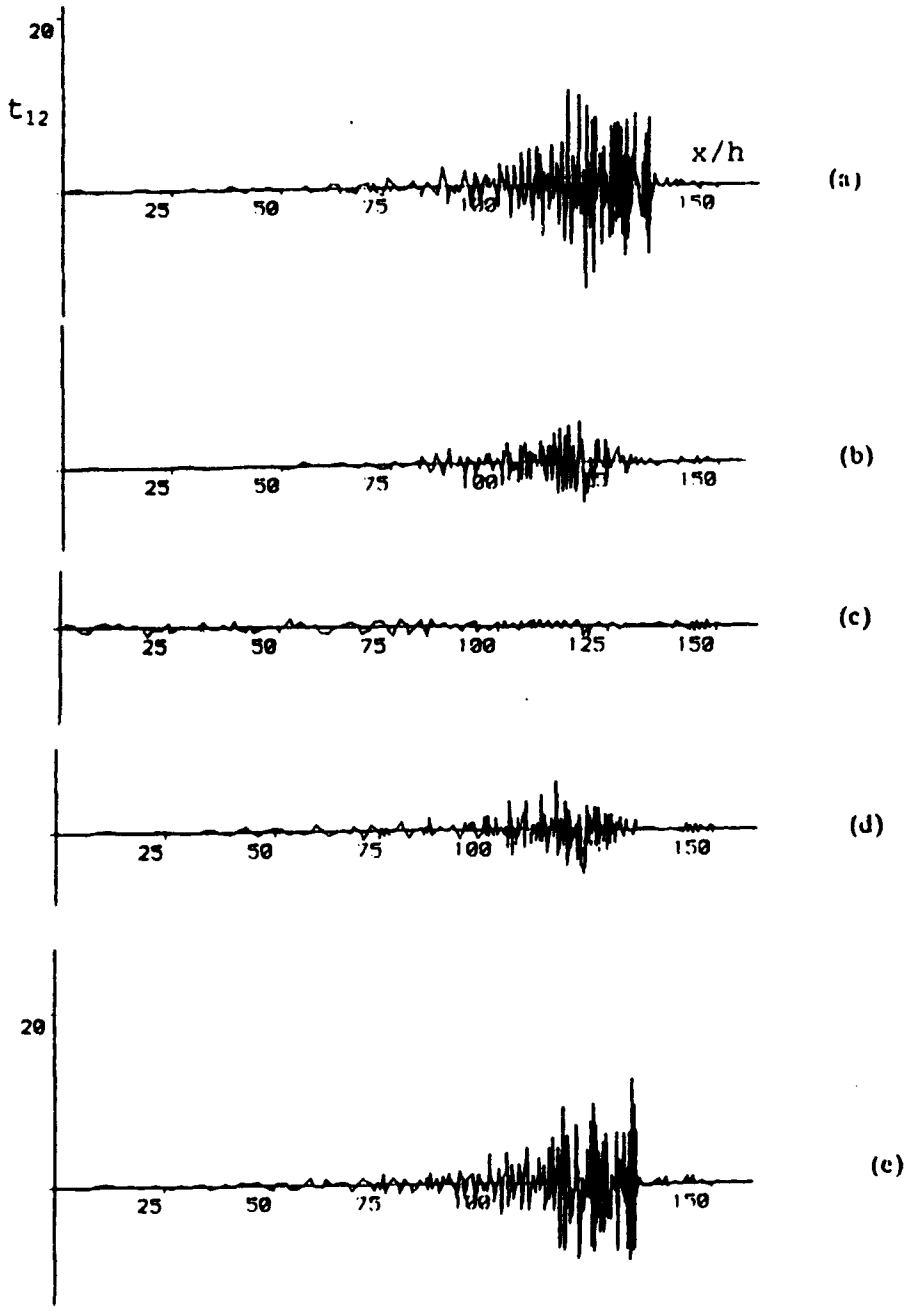

Figure 6 Stress component t_{12} in 4-ply plate at time $t = 200h/c_1$ for $\gamma = 60^0$ at:
(*a*) upper surface (*b*) upper interface (*c*) mid-surface
(*d*) lower interface (*e*) lower surface

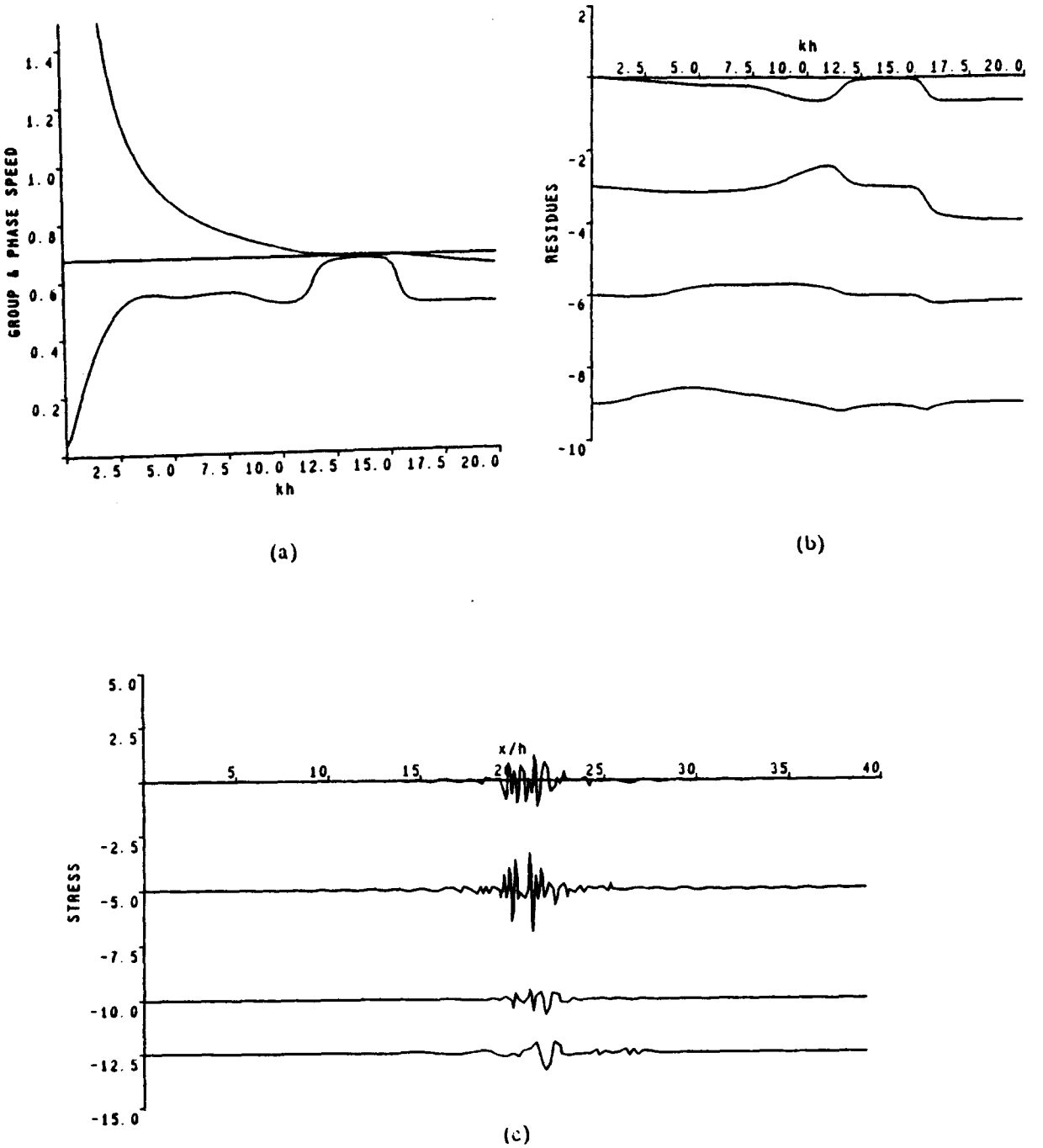

Figure 7 (a) Phase velocity (upper curve) and group velocity (lower curve) for branch 5 antisymmetric motion at $\gamma = 30^0$

(b) Residue contributions for branch 5 antisymmetric motion at $\gamma = 30^0$ (for details see text)

(c) Stress contributions for branch 5 antisymmetric motion at $\gamma = 30^0$ (for details see text)

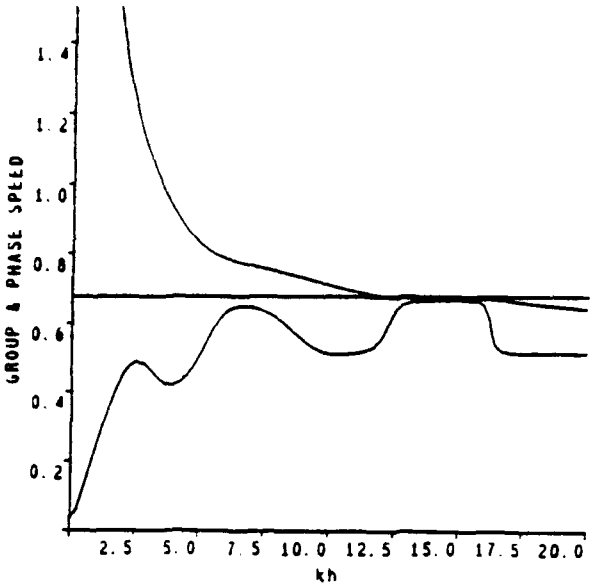

(a)

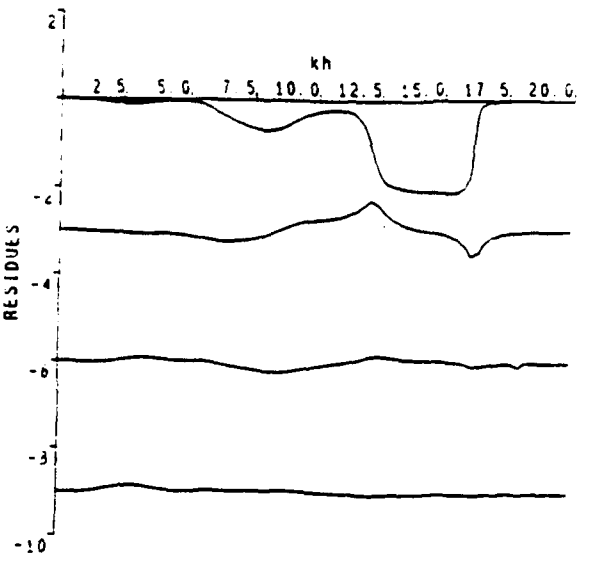

(b)

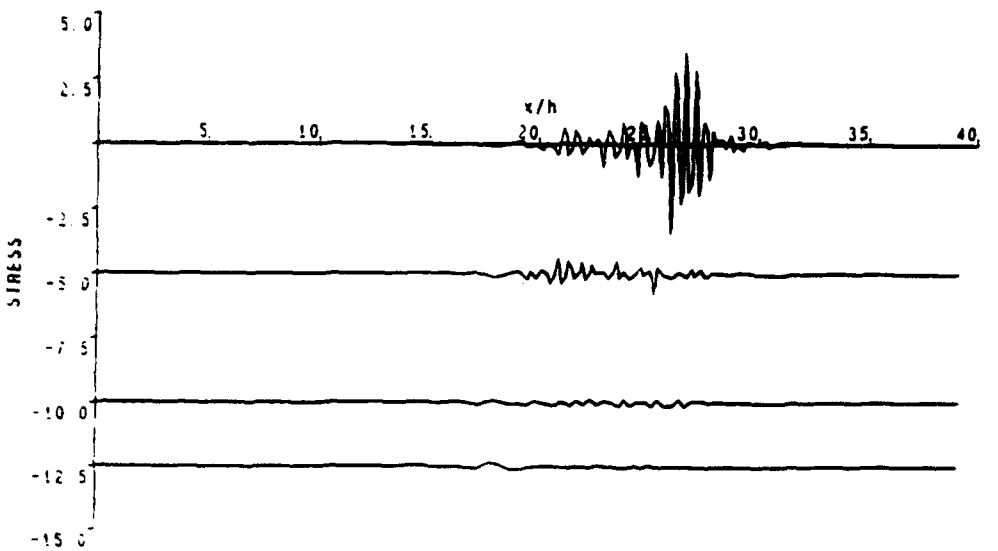

(c)

Figure 8 (a) Phase velocity (upper curve) and group velocity (lower curve) for branch 5 antisymmetric motion at $\gamma = 60^0$

(b) Residue contributions for branch 5 antisymmetric motion at $\gamma = 60^0$ (for details see text)

(c) Stress contributions for branch 5 antisymmetric motion at $\gamma = 60^0$ (for details see text)

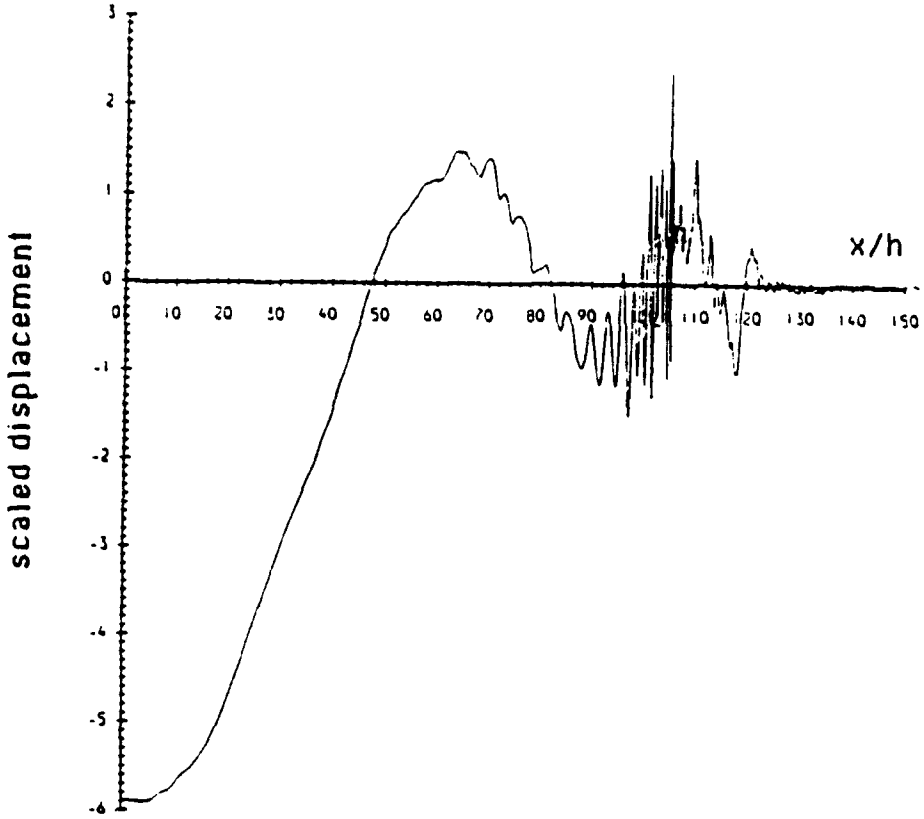

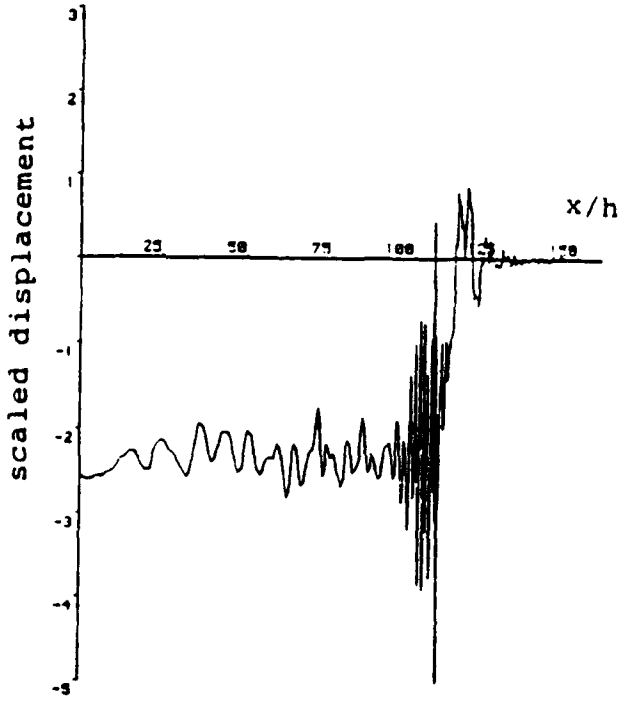

Figure 9 Upper surface normal displacement in 4-ply plate at time $t = 200h/c_1$, $\gamma = 30^0$. (*a*) Extensible model. (*b*) Inextensible model

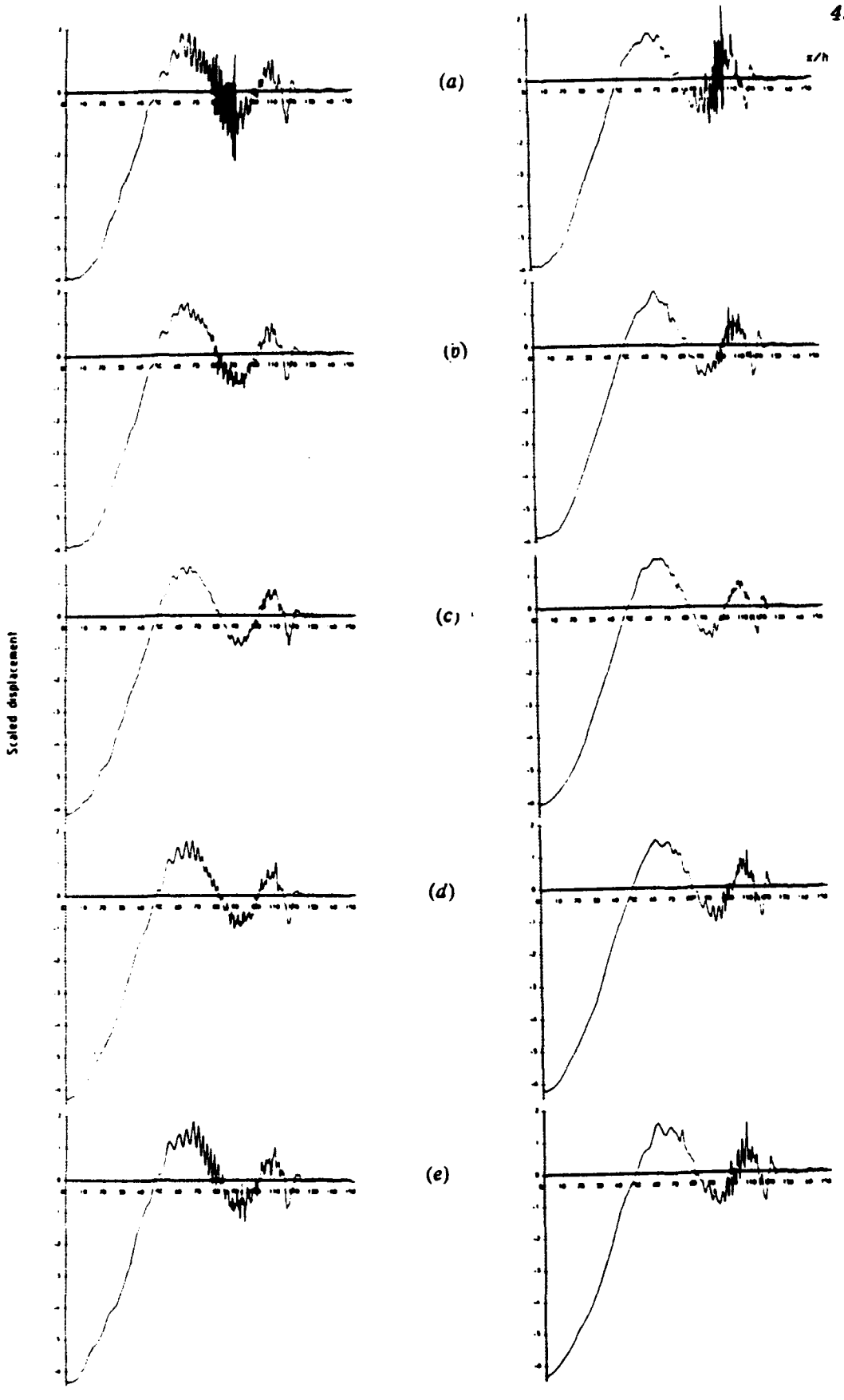

Figure 10 $\gamma = 0^0$:

Figure 11 $\gamma = 30^0$:

Normal displacement in 4-ply plate at time $t = 200h/c_1$.

Extensible model (*a*) upper surface, (*b*) upper interface

(*c*) midplane (*d*) lower interface (*e*) lower surface

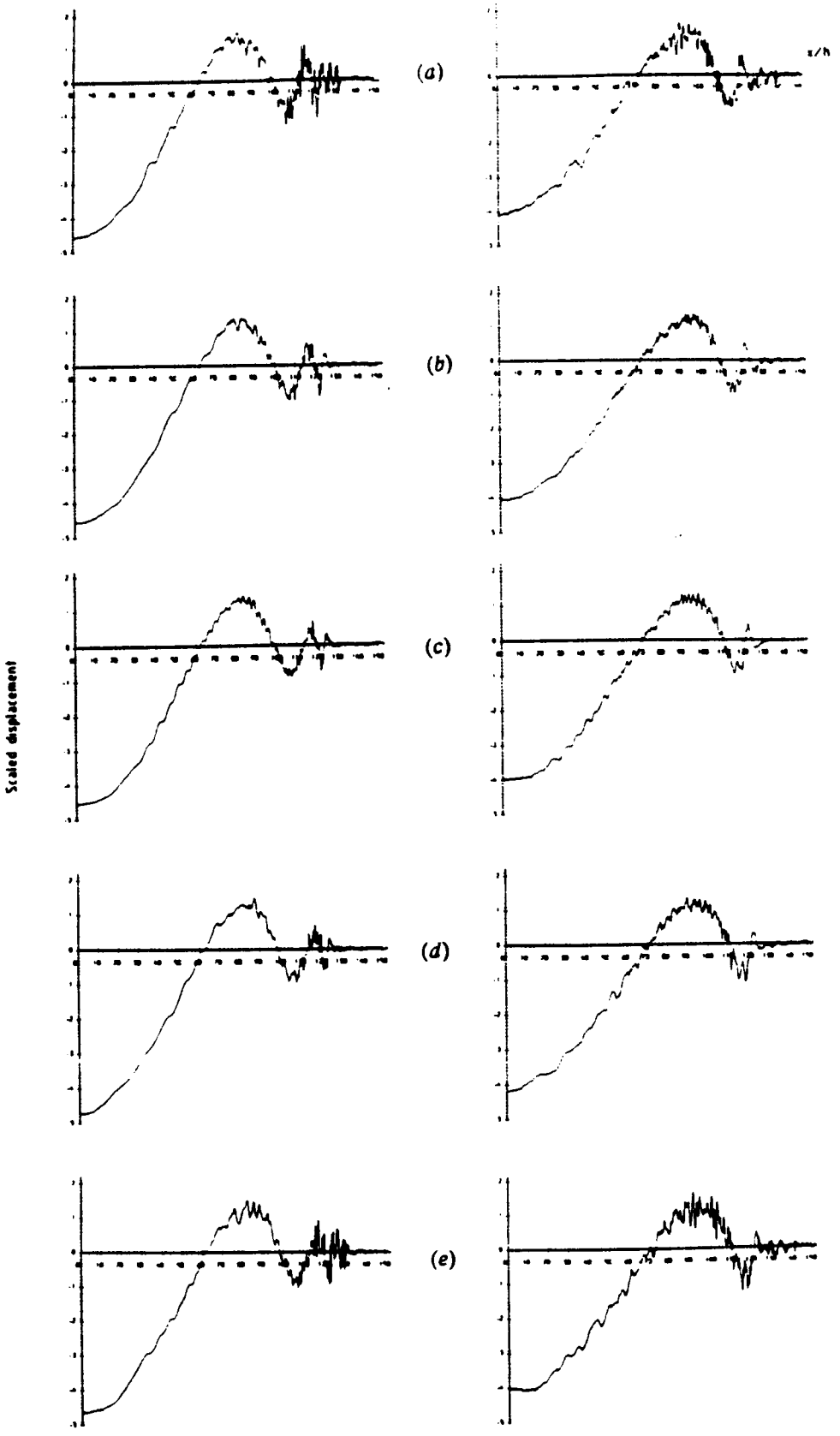

Figure 12 $\gamma = 60°$:

Figure 13 $\gamma = 90°$:

Normal displacement in 4-ply plate at time $t = 200h/c_1$.
Extensible model (*a*) upper surface. (*b*) upper interface
(*c*) midplane (*d*) lower interface (*e*) lower surface

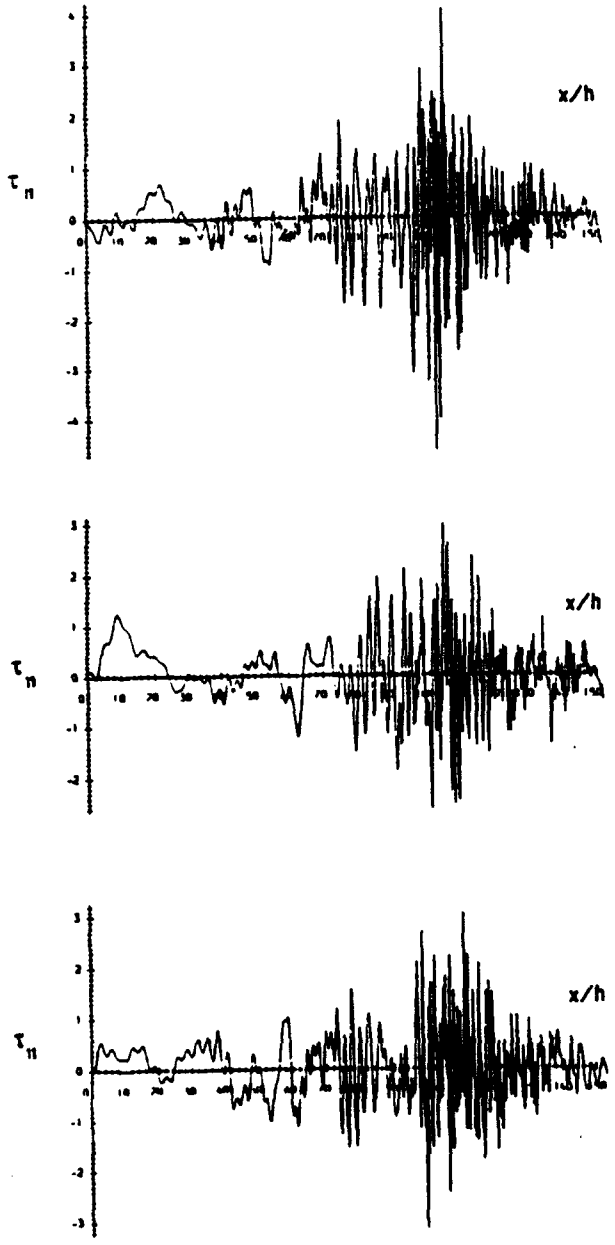

Figure 14 $\gamma = 30^0$:

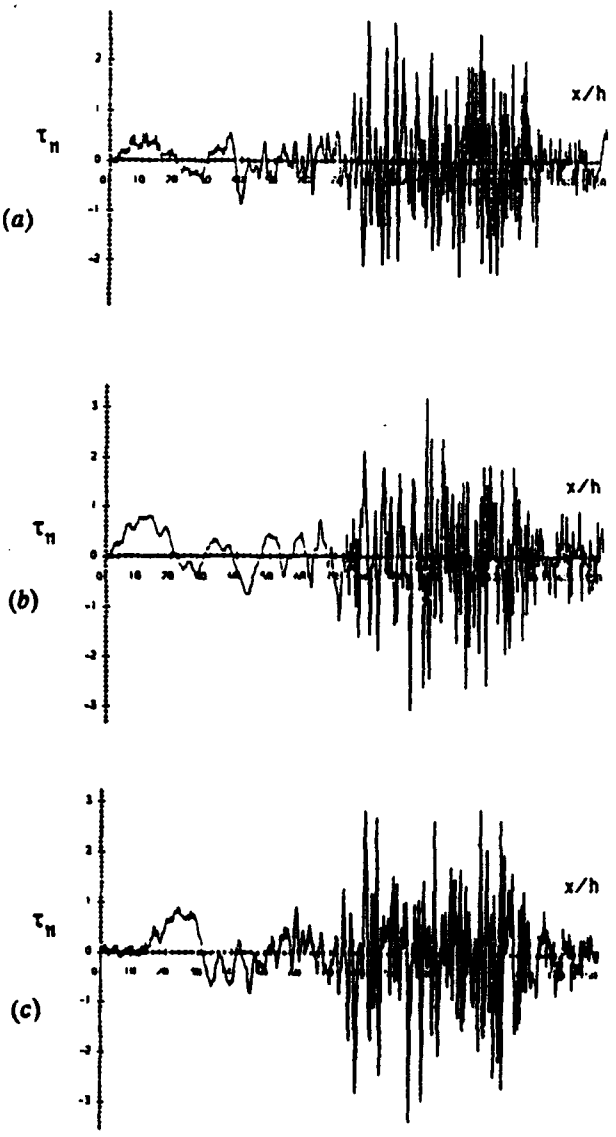

Figure 15 $\gamma = 60^0$:

Normal stress component t_{11} in 4-ply plate at time $t = 200h/c_1$.
Extensible model (*a*) upper interface (*b*) midplane
(*c*) lower interface

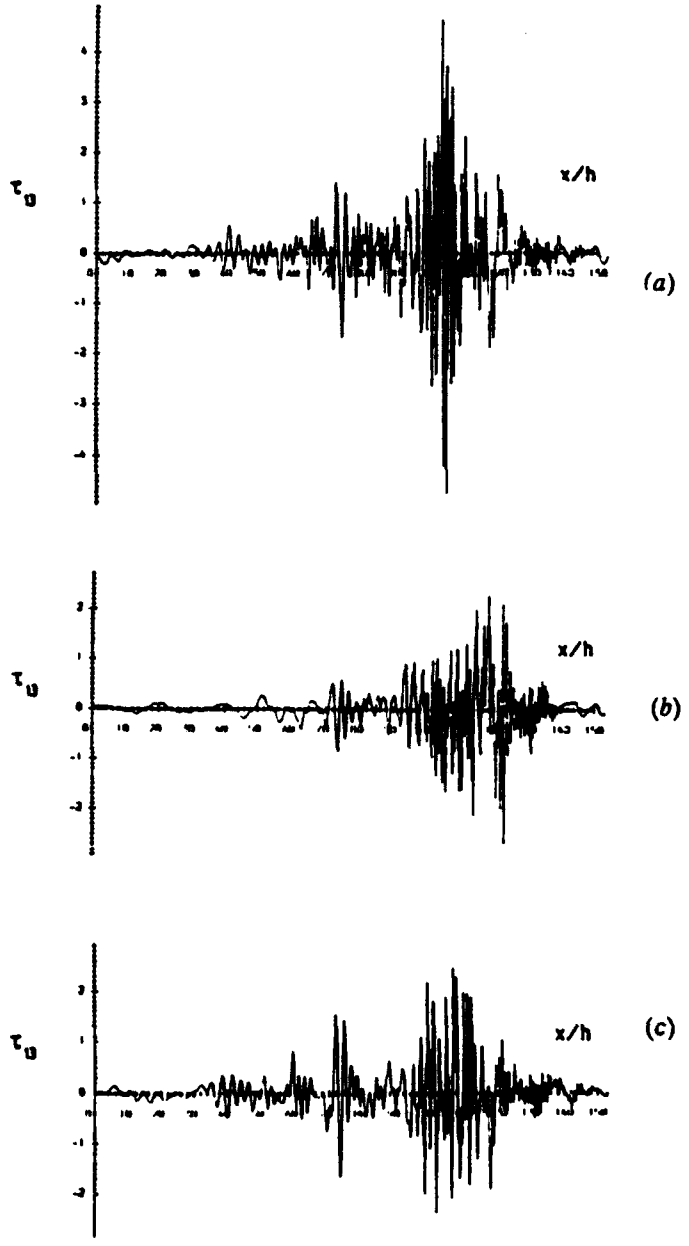

Figure 16 $\gamma = 30^0$:

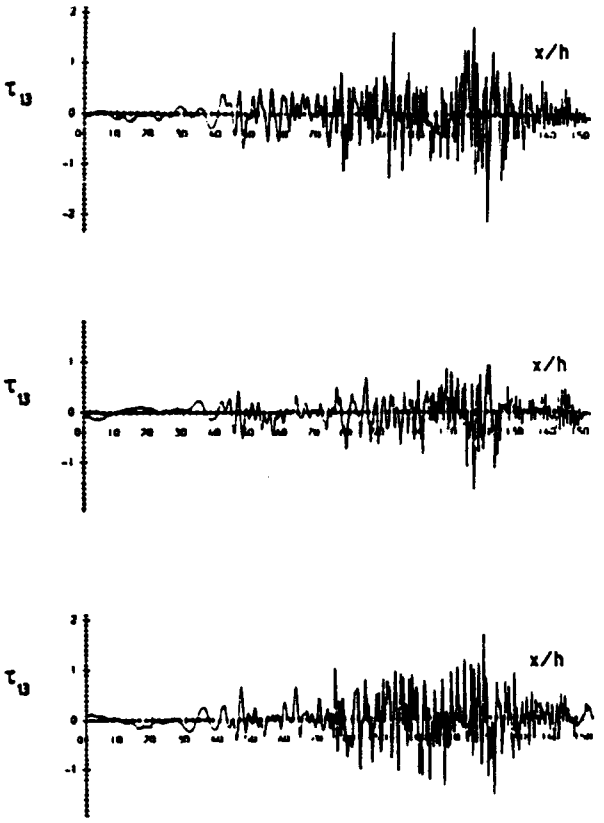

Figure 17 $\gamma = 60^0$:

Shear stress component t_{13} in 4-ply plate at time $t = 200h/c_1$,
Extensible model (*a*) upper interface (*b*) midplane
(*c*) lower interface

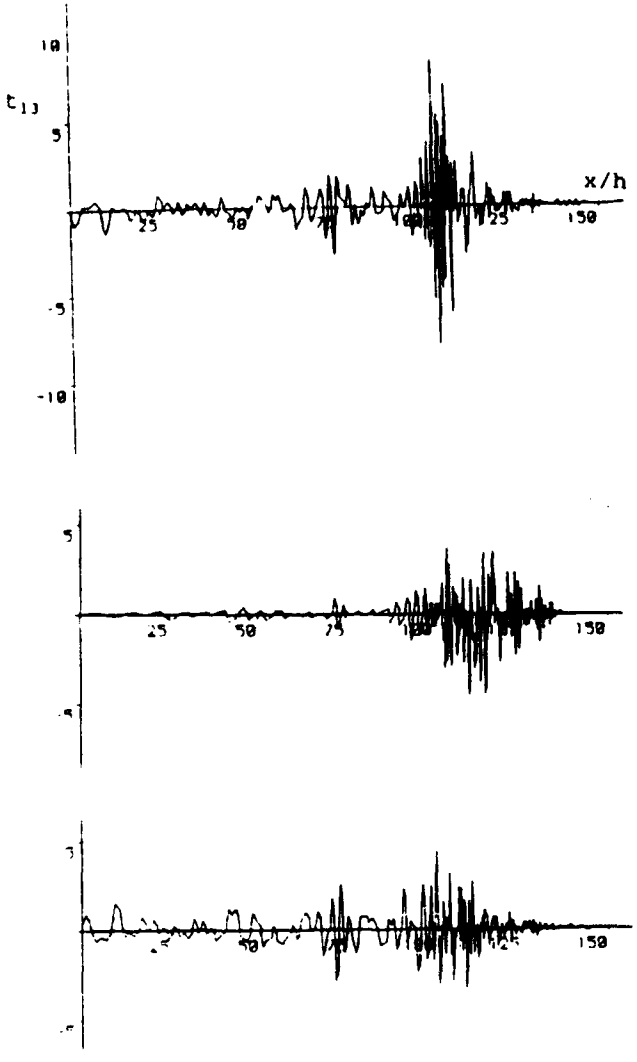

Figure 18 $\gamma = 30^0$:

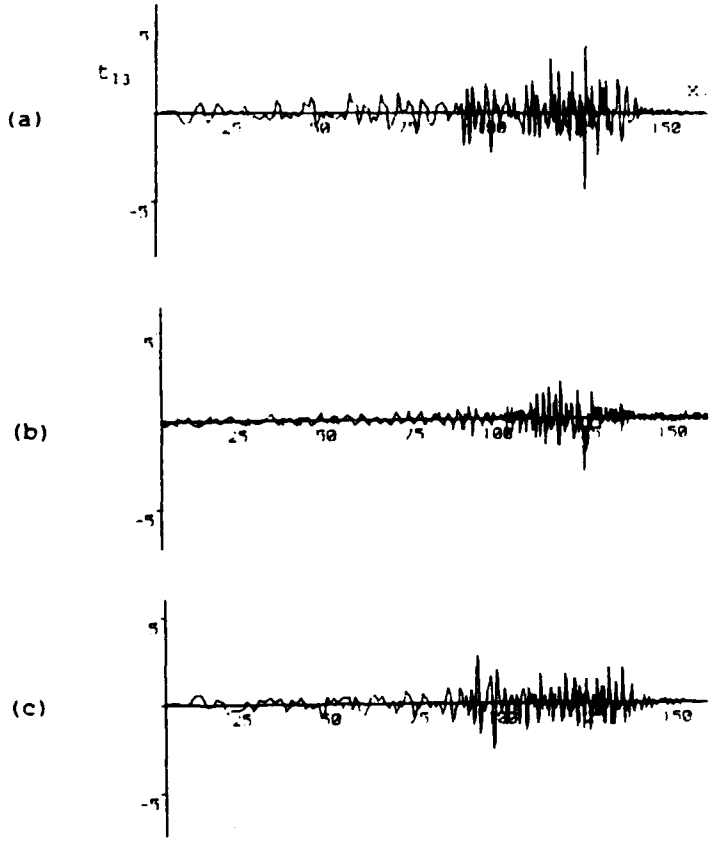

Figure 19 $\gamma = 60^0$:

Shear stress component t_{13} in 4-ply plate at time $t = 200h/c_1$,
Inextensible model (*a*) upper interface (*b*) mid-surface
(*c*) lower interface

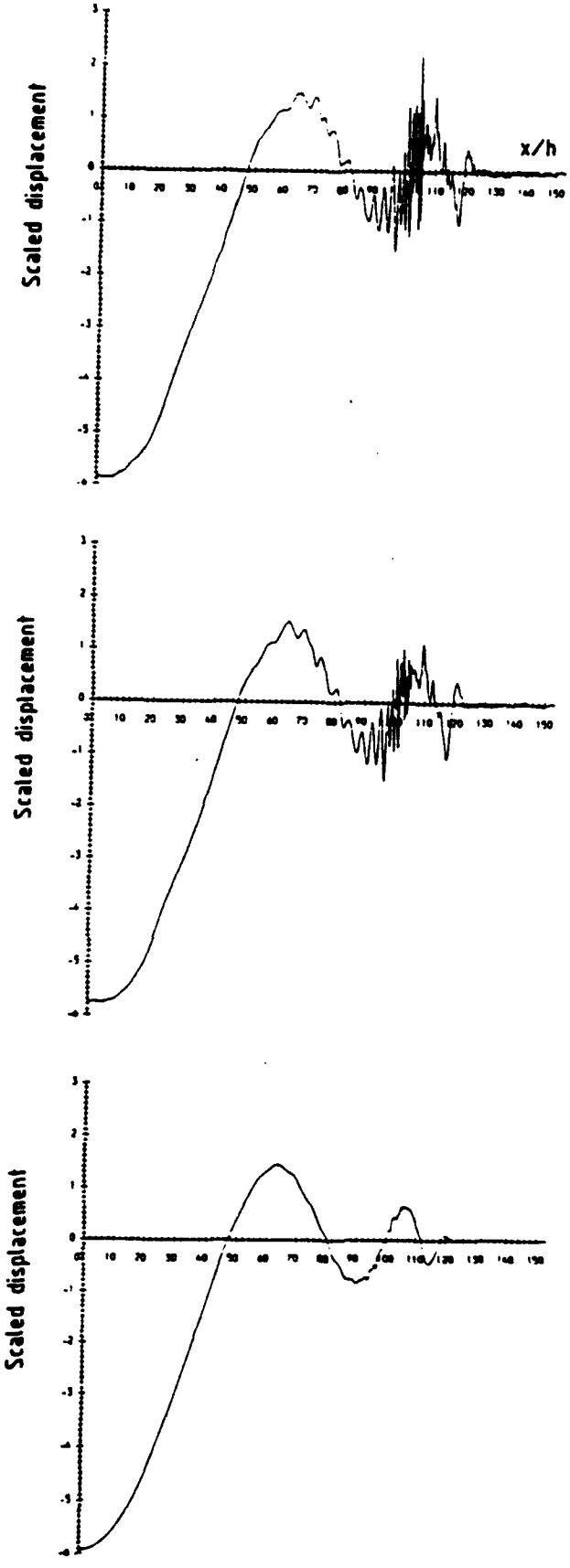

Figure 20 Upper surface normal displacement in 4-ply plate at time $t = 200h/c_1$. $\gamma = 30^0$: Extensible model. Square pulse impact of duration :
(*a*) $0.1h/c_1$. (*b*) $1.0h/c_1$. (*c*) $10.0h/c_1$.

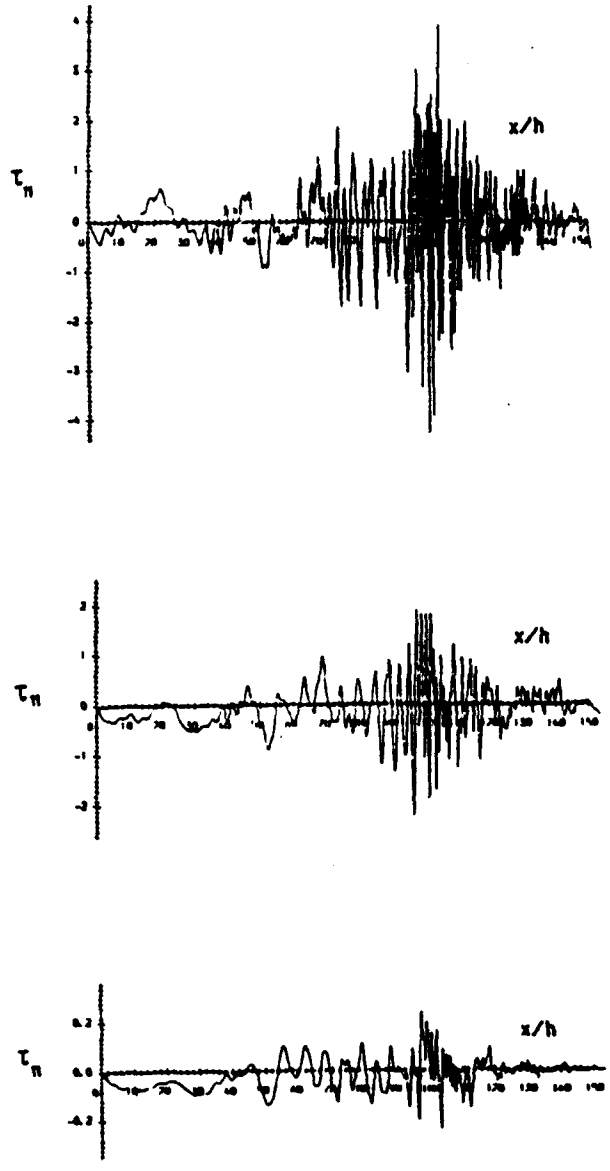

Figure 21 Upper interface normal stress component τ_{11} in 4-ply plate at time $t = 200h/c_1$, $\gamma = 30^0$: Extensible model. Square pulse impact of duration : (*a*) $0.1h/c_1$. (*b*) $1.0h/c_1$. (c) $10.0h/c_1$.

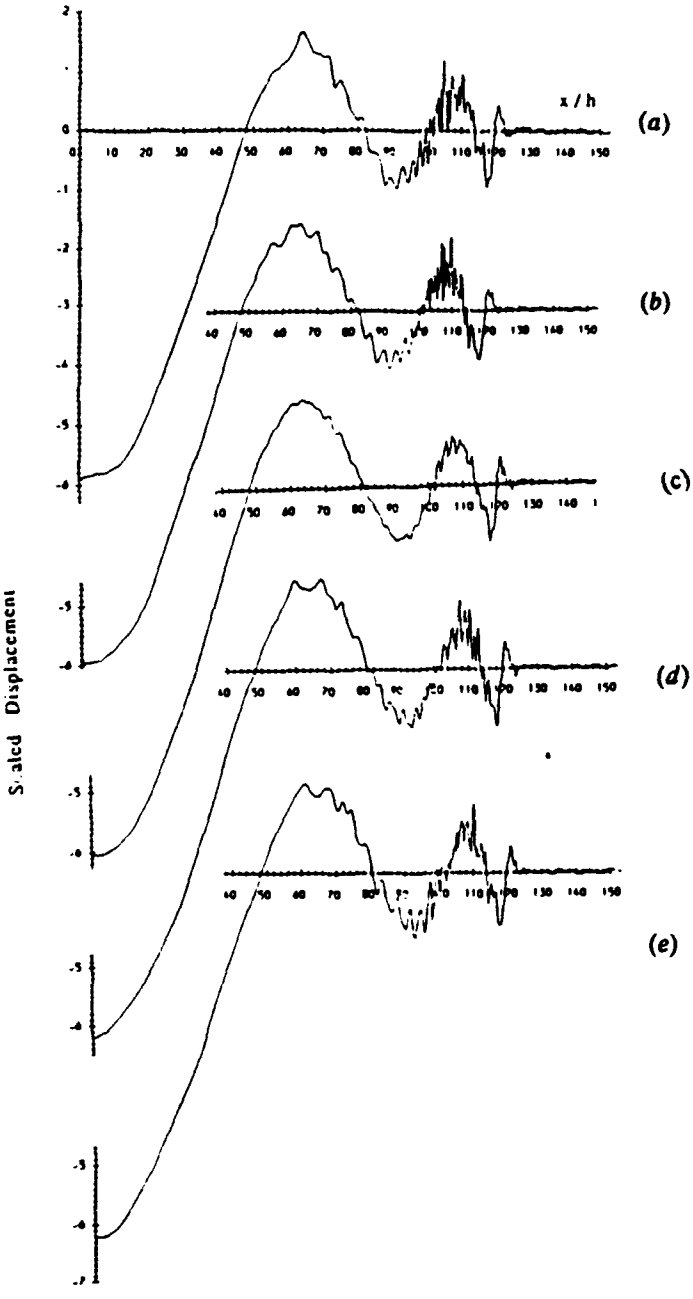

Figure 22 $\gamma = 30^0$

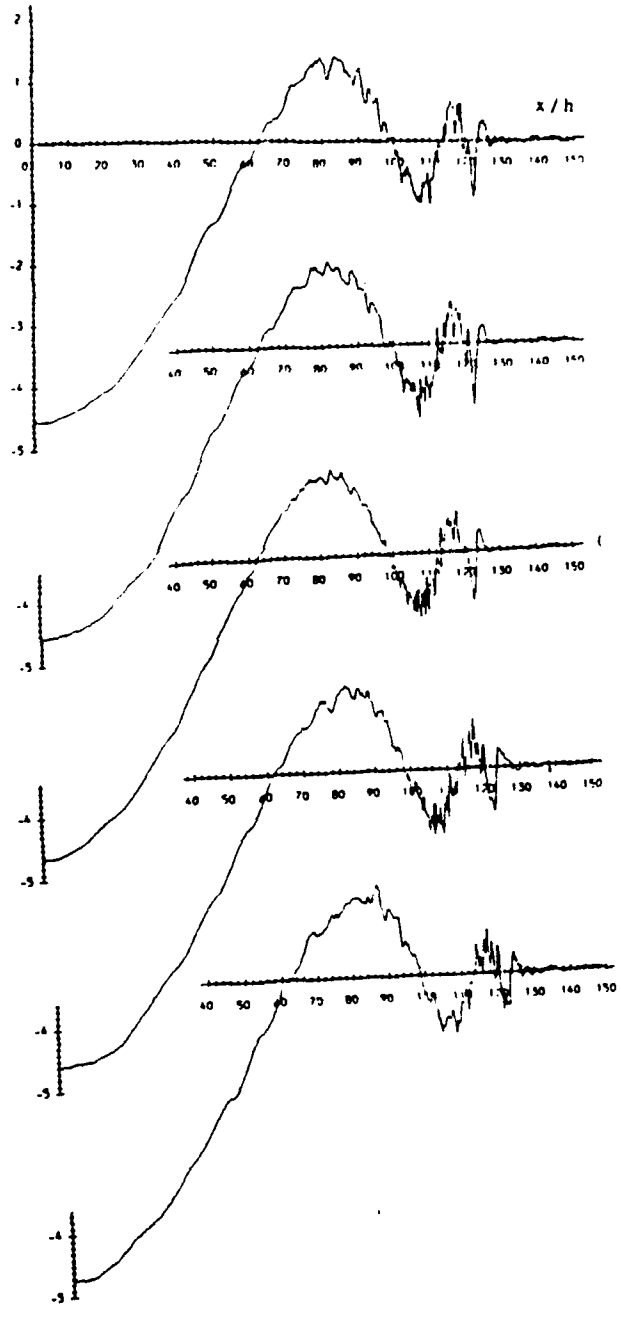

Figure 23 $\gamma = 60^0$

Normal displacement in 4-ply plate at time $t = 200h/c_t$, .
delta function impulse acting on upper interface. Extensible model :
(*a*) upper surface (*b*) upper interface (*c*) midplane
(*d*) lower interface (*e*) lower surface

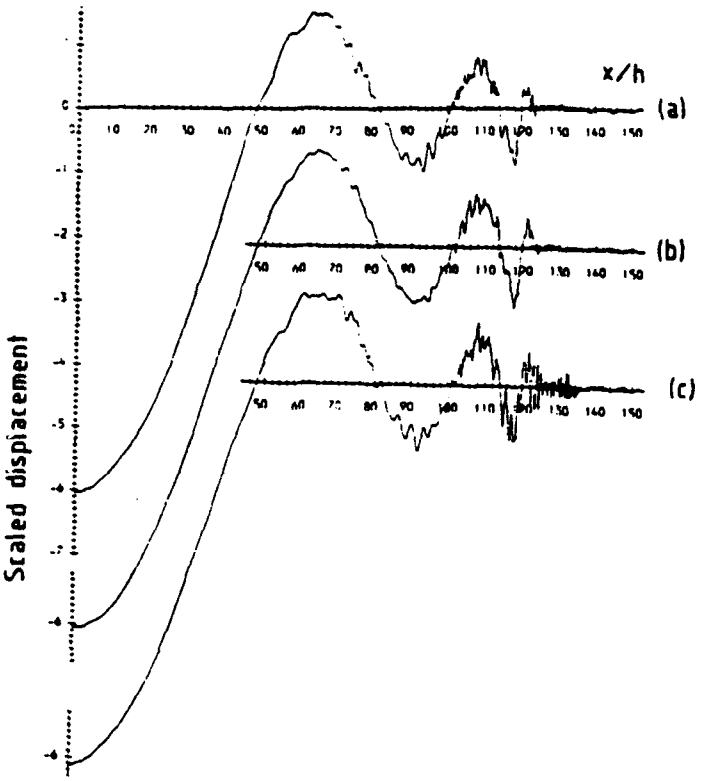

Figure 24 Normal displacement in 4-ply plate at time $t = 200h/c_1$, $\gamma = 30^0$: due to delta function impulse acting on midplane. Extensible model :
(*a*) upper surface (*b*) upper interface (*c*) midplane
By symmetry, lower surface = (*a*), lower interface = (*b*)

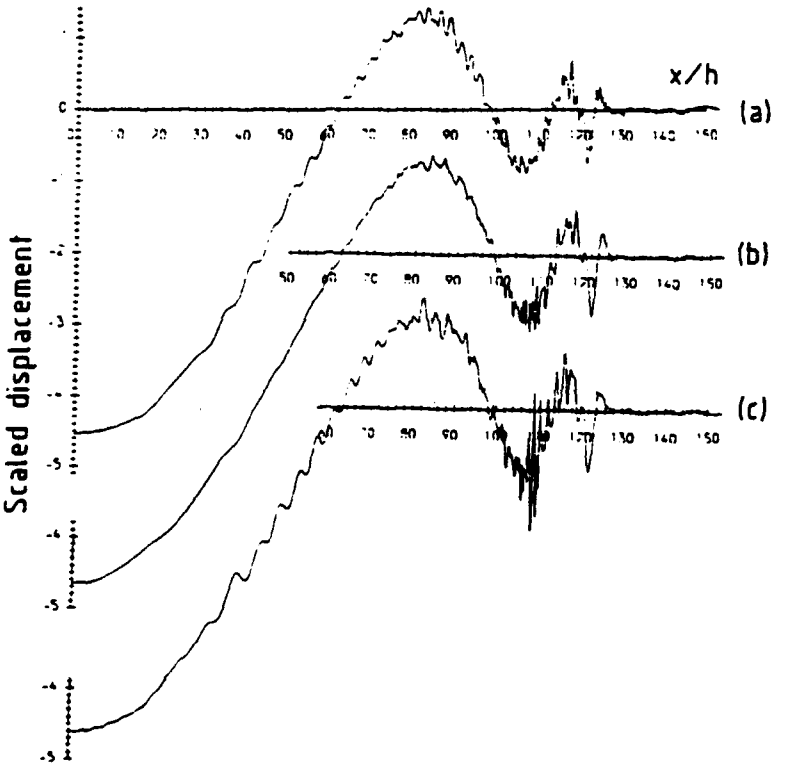

Figure 25 Normal displacement in 4-ply plate at time $t = 200h/c_1$, $\gamma = 60^0$: due to delta function impulse acting on midplane. Extensible model :
(*a*) upper surface (*b*) upper interface (*c*) midplane
By symmetry, lower surface = (*a*), lower interface = (*b*)

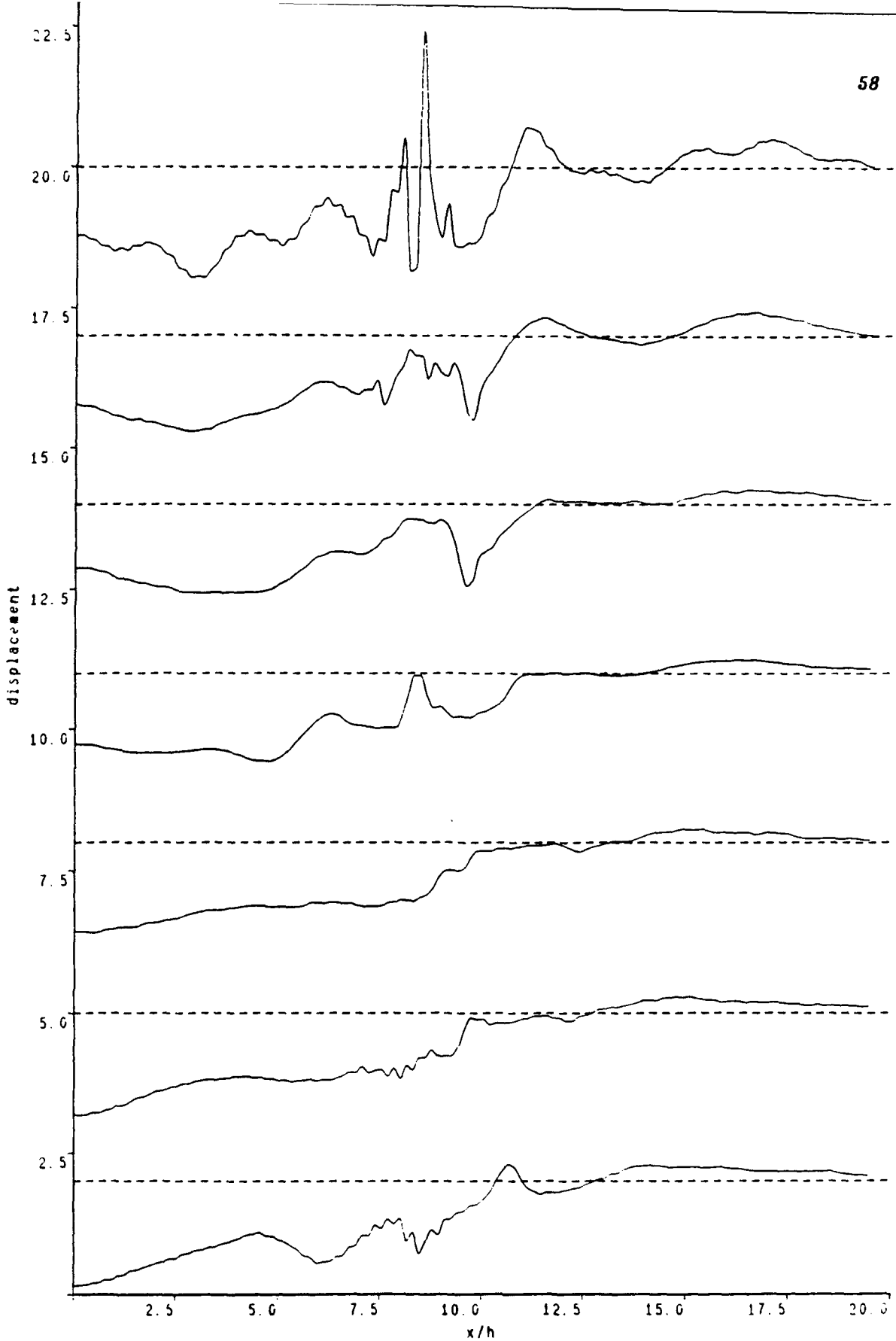

Figure 26 Normal displacement in 6-ply plate at time $t = 20\ h/c_1$, $\gamma = 90^0$:
Extensible model : (*a*) upper surface (*b*) outer upper interface
(*c*) inner upper interface (*d*) midplane (*e*) inner lower interface
(*f*) outer lower interface (*g*) lower surface

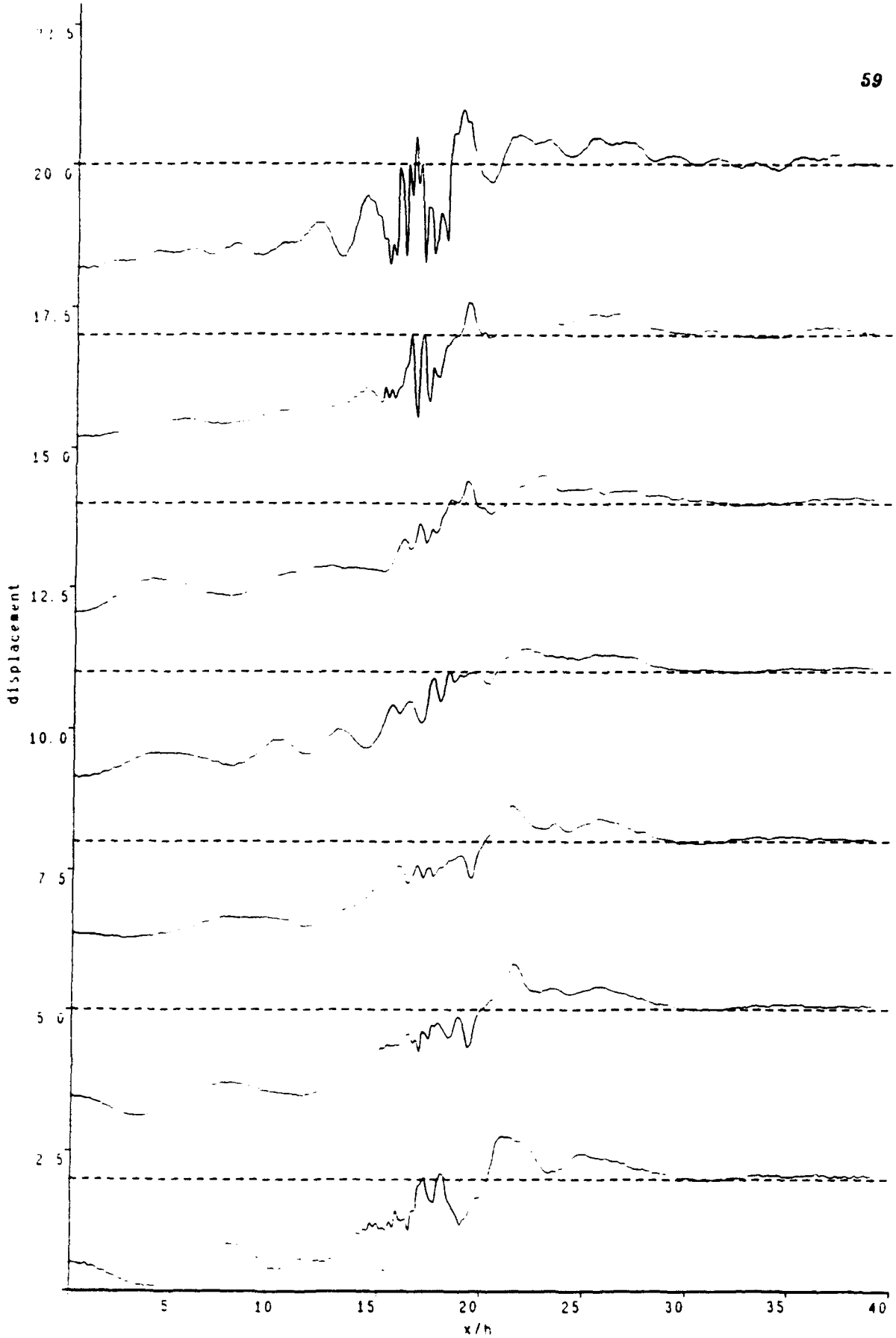

Figure 27 Normal displacement in 6-ply plate at time $t = 40h/c_1$, $\gamma = 90°$:
Extensible model : (*a*) upper surface (*b*) outer upper interface
(*c*) inner upper interface (*d*) midplane (*e*) inner lower interface
(*f*) outer lower interface (*g*) lower surface

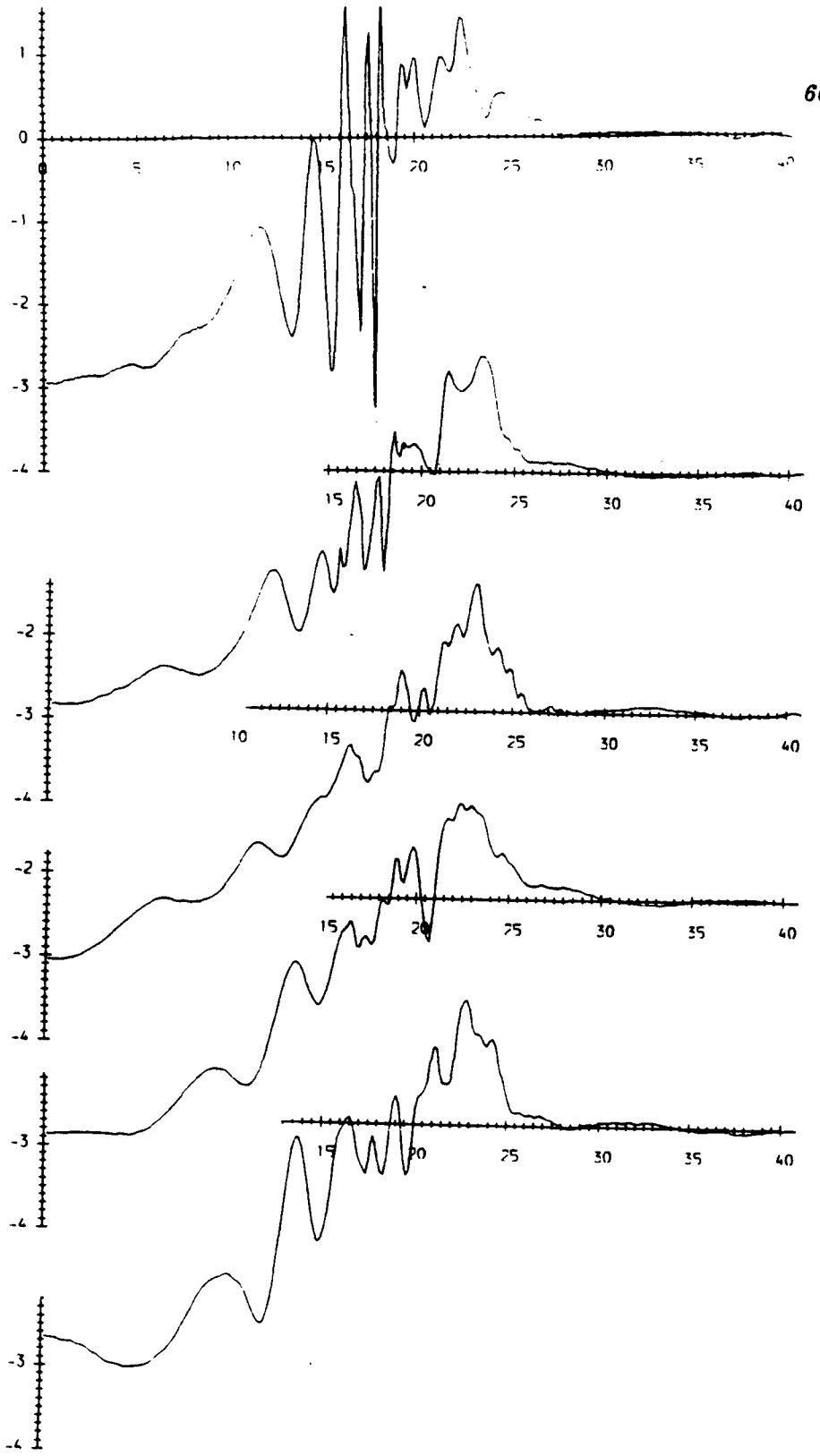

Figure 28 Normal displacement in 4-ply plate at time $t = 40h/c_1$, $\gamma = 0^0$:
Extensible model : (*a*) upper surface (*b*) upper interface
(*c*) midplane (*d*) lower interface (*e*) lower surface

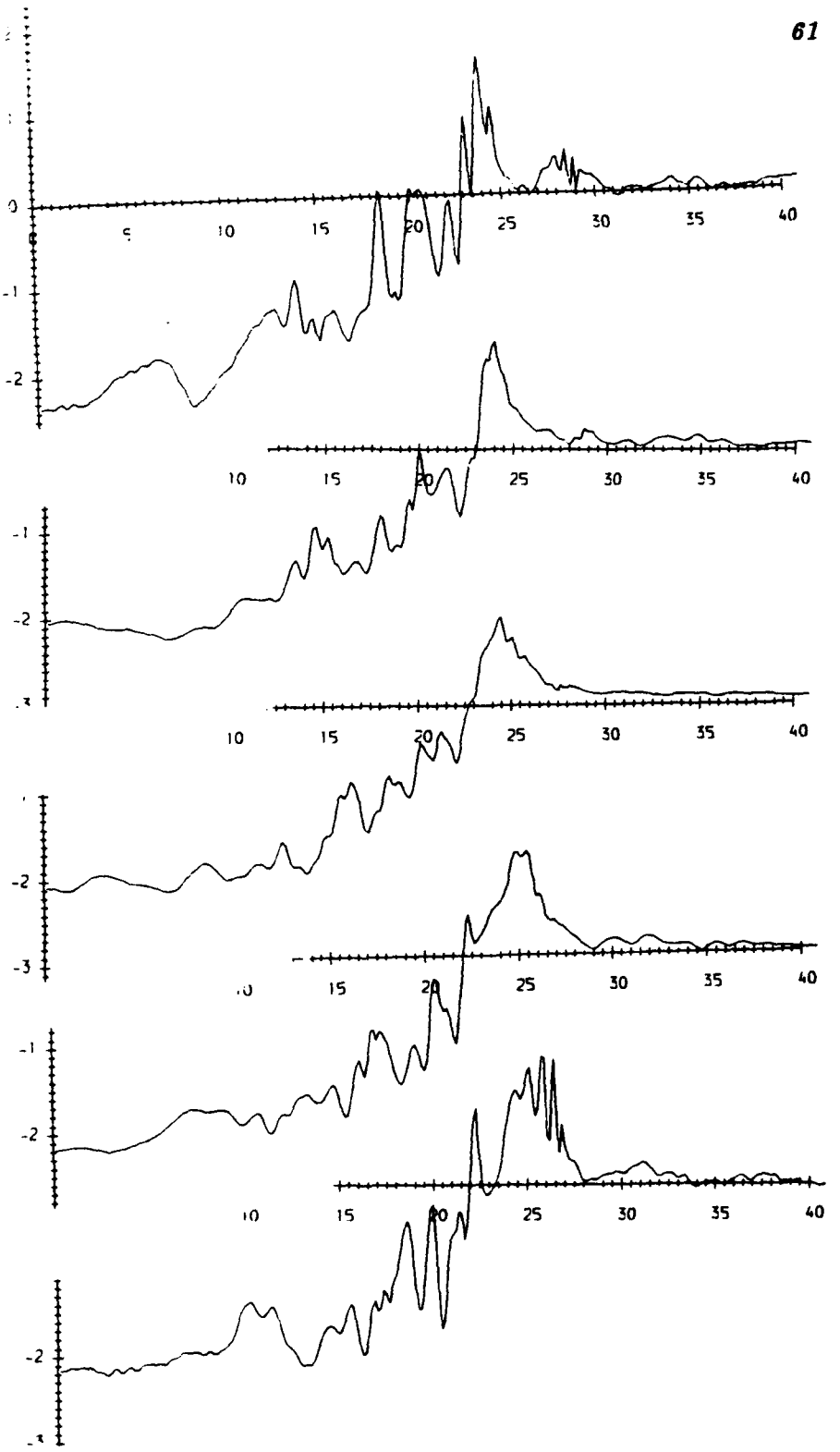

Figure 29 Normal displacement in 4-ply plate at time $t = 40h/c_1$, $\gamma = 90^0$:
Extensible model : (*a*) upper surface (*b*) upper interface
(*c*) midplane (*d*) lower interface (*e*) lower surface

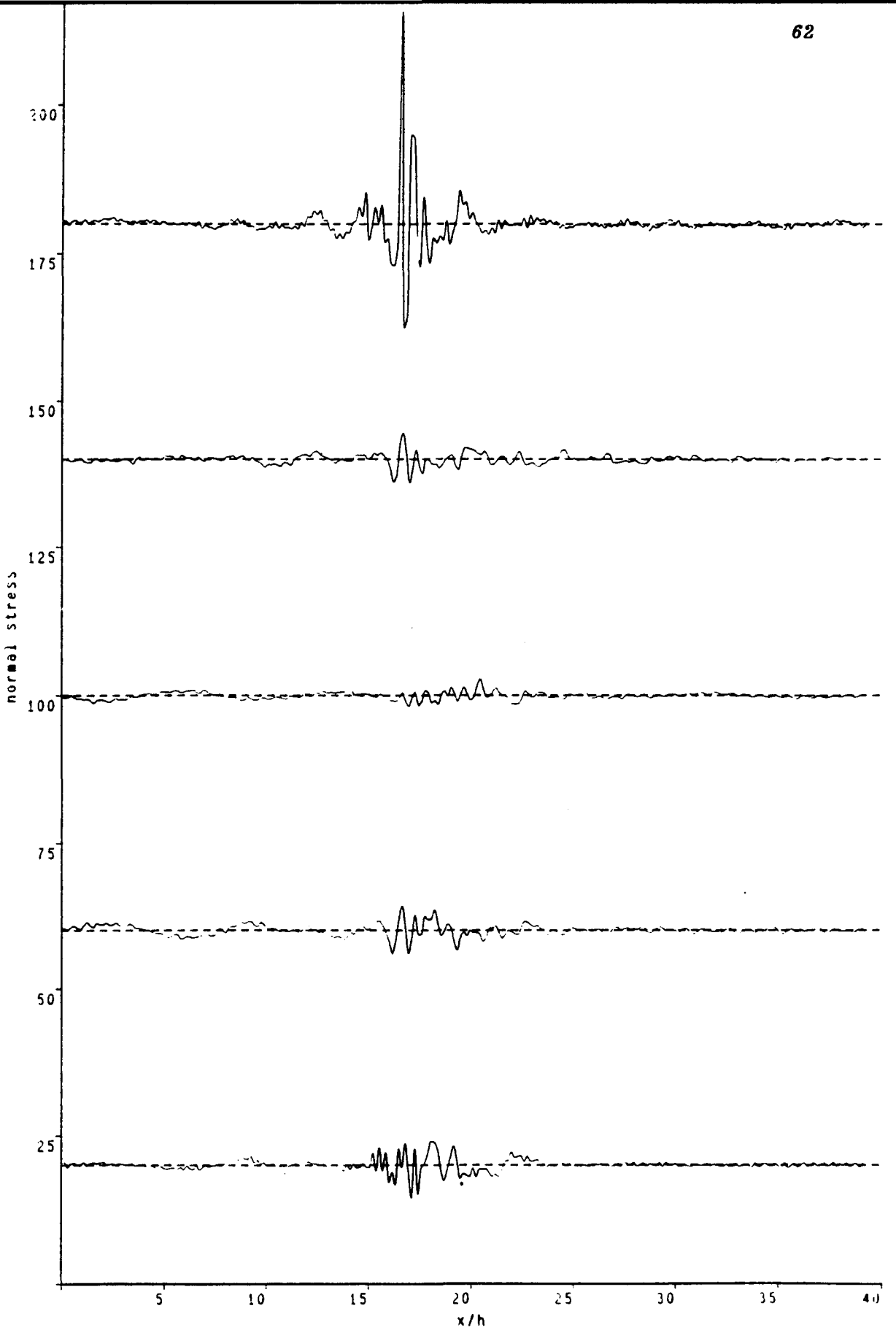

Normal stress component t_{33} in 6-ply plate at time $t = 40h/c_1$, $\gamma = 90°$: Extensible model

Figure 30

(a) outer upper interface
(b) inner upper interface (c) midplane
(d) inner lower interface (e) outer lower surface

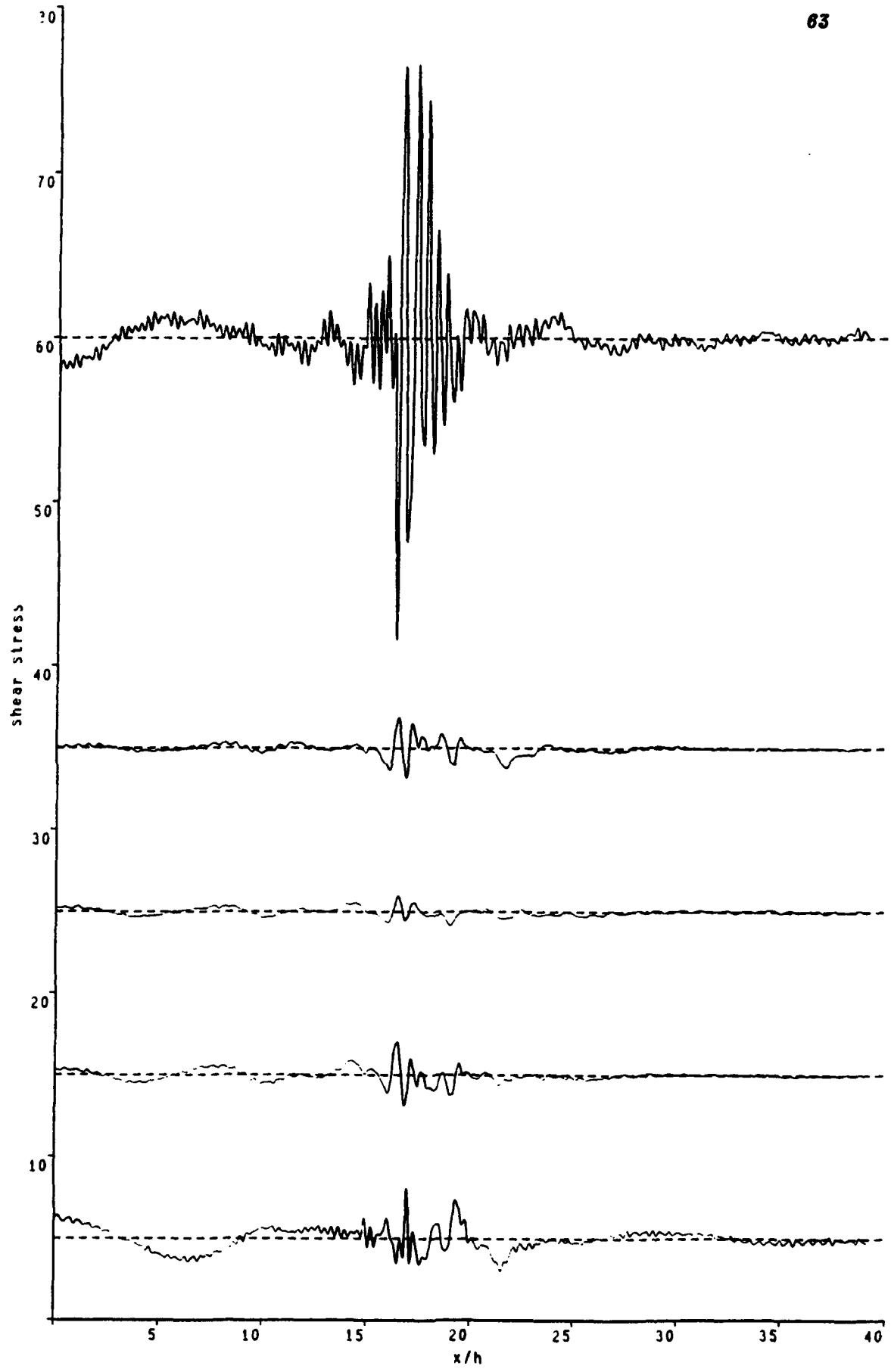

Shear stress component t_{13} in 6-ply plate at time $t = 40h/c_1$, $\gamma = 90°$: Extensible model:

Figure 31

(a) outer upper interface
(b) inner upper interface

☆ U.S. Government Printing Office:1992—648-127/62433